The histone methyltransferase DOT1L is essential for humoral immune responses.

Liam Kealy[1,2], Andrea Di Pietro[1,2], Sebastian Scheer[1,2], Lennard Dalit[3,4], Joanna R Groom[3,4], Colby Zaph[1,2] and Kim L Good-Jacobson[1,2].

[1]Department of Biochemistry and Molecular Biology, Monash University, Clayton, Victoria 3800, Australia; [2]Infection and Immunity Program, Biomedicine Discovery Institute, Monash University, Clayton, Victoria 3800, Australia. [3]Divisions of Immunology and Molecular Immunology, Walter and Eliza Hall Institute of Medical Research, Parkville, Victoria 3052, Australia. [4]Department of Medical Biology, University of Melbourne, Parkville, Victoria 3010, Australia.

Correspondence should be addressed to Kim Good-Jacobson

ORCID: orcid.org/0000-0003-1891-7274

Department of Biochemistry and Molecular Biology

Monash University

15 Innovation Walk

Clayton, Victoria 3800 Australia

Phone: (+613) 990-29510

Email: kim.jacobson@monash.edu

Twitter: @KimLJacobson

Short running title: B cell responses require DOT1L.

Abbreviations used: AID – activation-induced cytidine deaminase; ASCs – antibody-secreting cells; BCL6 – B cell lymphoma-6; CPM – counts per million; CTV – cell trace violet; DOT1L – disruptor of telomeric silencing 1-like, EZH2 – enhancer of zeste homolog 2; FVS – fixable viability stain; H3K27me3 – trimethylation of lysine 27 on histone H3; Ig – immunoglobulin; KLH – Keyhole Limpet Hemocyanin; MLLr-ALL – Mixed Lineage Leukaemia-rearranged acute lymphoblastic leukaemia; NP – (4-Hydroxy-3-nitrophenyl)-acetyl; PRC2 – polycomb repressive complex 2; S1PR - sphingosine-1-phosphate receptor; Th cells – T helper cells.

ABSTRACT

Histone modifiers are essential molecular regulators that underpin the ability of immune cells to reprogram their gene expression during differentiation. The recruitment of the histone methyltransferase DOT1L induces oncogenic gene expression in a subset of B cell leukemia. Despite its importance, little is known about its role in the humoral immune system. Herein, we demonstrate that DOT1L is a critical regulator of B cell biology. *Dot1l*$^{f/f}$*Mb1*$^{Cre/+}$ mice had a block in B cell development, culminating in a significant reduction of mature B cells in the periphery. Upon immunization or influenza infection, germinal centers failed to form in *Dot1l*$^{f/f}$*Cd23*$^{Cre/+}$ mice. Consequently, immunized mice revealed that DOT1L was essential for the formation of B cell memory populations. *Dot1l* deletion significantly attenuated the formation of class-switched antibody-secreting cells in both T-dependent and T-independent responses. Transcriptome, pathway and histological analysis identified a key role for DOT1L in reprogramming gene expression for migration and localization during the initial stages of a humoral response. Together, these results demonstrate an essential role for DOT1L in antigen-dependent B cell differentiation and hence, in generating an effective and lasting humoral immune response.

Keywords: B cells; antibody; epigenetics; DOT1L; humoral responses; H3K79

INTRODUCTION

A successful antibody-mediated immune response leads to pathogen clearance and the formation of immune memory. These processes underpin the vast majority of vaccines (Good-Jacobson, 2018). The foundation for this success originates from the activation of a small number of antigen-specific naïve B cells. After activation, B cell differentiation is instructed by specific molecular programs that regulate fate and function during an immune response. These programs are modulated by epigenetic regulators (e.g. histone modifiers, siRNAs, DNA methylases) and transcription factors working in concert to determine whether genes are activated or repressed (Zhang and Good-Jacobson, 2019). Histone modifiers regulate chromatin accessibility, thereby regulating the accessibility of transcriptional machinery to their targets (Strahl and Allis, 2000). Importantly, the same histone modifiers emerging as important regulators of B cell differentiation can also become dysregulated in malignancies (Alberghini et al., 2015; Beguelin et al., 2013; Inaba et al., 2013). Thus, histone modifiers are therapeutically attractive to target with small molecule inhibitors (Arrowsmith et al., 2012). It is therefore important to understand the roles of histone modifiers in regulating B cell differentiation in both primary and secondary lymphoid organs.

DOT1L (*Disruptor of Telomeric Silencing 1-Like*) is the sole known enzyme that methylates lysine 79 of histone H3 (H3K79), and is most well-known for its role in oncogenesis. Approximately 40% of pediatric leukemias have been linked to H3K79 methylation-mediated oncogenic gene expression (Worden et al 2019). B cell Acute Lymphoblastic Leukemia (B-ALL) is an aggressive malignancy that affects children and adults, with long-term survival rates of <40% (Geng et al., 2012). A prominent subtype is *MLL* (*Mixed Lineage Leukaemia*)-rearranged B-ALL (*MLL*r B-ALL), The defining feature of *MLL*r-ALLs is rearrangement of the epigenetic regulator *MLL*,

which results in the binding of MLL with any one of over 50 fusion partners. While this promiscuous partnering makes it difficult to find genuine therapeutic targets, another prominent feature of this leukaemia is the recruitment of a second epigenetic regulator, DOT1L (Krivtsov et al., 2008; Okada et al., 2005). Malignant gene expression is driven by DOT1L activity: inactivation of DOT1L downregulates genes targeted by MLL-fusion protein complexes (Bernt et al., 2011). Thus, DOT1L inhibition has become a major focus of translational research and is now in phase I/II clinical trials. Despite the clear importance of this molecule, there is scant information on the role of DOT1L in lymphocyte development in primary lymphoid organs or differentiation during an immune response in the periphery.

Epigenetic regulation of B cell differentiation is a nascent field, with understanding mostly limited to the roles of the methyltransferases EZH2 (Beguelin et al., 2013; Caganova et al., 2013), MLL2 (Zhang et al., 2015), demethylase LSD1 (Good-Jacobson, 2019; Haines et al., 2018; Hatzi et al., 2019) and acetyltransferase MOZ (Good-Jacobson et al., 2014) in germinal center (GC) biology. DOT1L was recently found to be expressed by human tonsillar and lymph node GC B cells (Szablewski et al., 2018). Differential H3K79 methylation on the *IgH* locus in plasma cells compared to B cells has been hypothesized to mediate the transition from membrane-bound to secretory forms of immunoglobulin (Milcarek et al., 2011). Thus, given its prominent role in *MLL*r B-ALL, its expression by GC B cells and potential role in antibody production, we set out to investigate the function of DOT1L in B cell differentiation and function.

By generating novel mouse strains deficient in DOT1L in either developing B cells or mature B cells, we describe previously unknown functional roles for DOT1L in B cell differentiation in both

primary and secondary lymphoid organs. Our experiments delineate DOT1L as a vital checkpoint molecule during an immune response, as evidenced by the complete abrogation of immune responses to a range of immunization and infection models. In particular, our study links histone modification to the regulation of a network of migration-related genes and ultimately, B cell positioning in the follicle. Together, these results reveal the absolute requirement for DOT1L for B cells to mount an effective immune response in vivo.

RESULTS AND DISCUSSION

DOT1L is required for B cell development

We first sought to determine whether DOT1L was required in B cell biology through the generation of *Dot1l*$^{f/f}$*Mb1*$^{Cre/+}$ mice in which exon 2 of *Dot1l* was excised upon *Igα* expression (Figure S1A). Spleens from *Dot1l*$^{f/f}$*Mb1*$^{Cre/+}$ mice were notably smaller than those from *Mb1*$^{Cre/+}$ control mice (Figures S1B-S1C), and the B cell population was significantly reduced in *Dot1l*$^{f/f}$*Mb1*$^{Cre/+}$ mice compared to both *Dot1l*$^{f/+}$*Mb1*$^{Cre/+}$ and *Mb1*$^{Cre/+}$ controls (Figure S1D). Histological analyses revealed DOT1L-deficient mice were able to form follicular structures, however a thinner marginal zone structure was clearly evident (Figure S1E). Correspondingly, both splenic marginal zone and follicular B cells were significantly decreased (Figures S1F-S1I). Furthermore, circulating antibodies of all isotypes were significantly decreased in the absence of DOT1L (Figures S1J-S1O).

Thus, it appeared that DOT1L was required for efficient production of B cells to populate secondary lymphoid organs such as the spleen. To investigate, the production of developing B cell subsets in the bone marrow of *Dot1l*$^{f/f}$*Mb1*$^{Cre/+}$ and *Dot1l*$^{f/+}$*Mb1*$^{Cre/+}$ were compared to *Mb1*$^{Cre/+}$ controls. Deficiency in DOT1L resulted in a clear decrease in the B cell population (Figure S1P). In keeping with the deletion of *Dot1l* at the pro-B cell stage in this conditional deletion, there was no significant change in either pre-pro B cells (data not shown) or pro-B cells (Figure S1Q). There was, however, a ~3-fold significant decrease in both the frequency (data not shown) and number (Figures S1Q) in all subsequent developing B cell subsets. Furthermore, in most instances, mice heterozygous for the floxed allele suggested a gene dosage effect of DOT1L during the development of B cells (Figure S1). These data demonstrate an essential requirement for DOT1L

during B cell development in the bone marrow and thus establishment of peripheral B cell populations.

DOT1L is essential for formation of GCs

DOT1L was recently found to be expressed in a subset of human GC B cells, suggesting a role for DOT1L in the GC (Szablewski et al., 2018). The significantly reduced number of peripheral B cells in *Dot1l*$^{f/f}$*Mb1*$^{Cre/+}$ mice made the precise role of DOT1L in antigen-driven responses difficult to disentangle from the developmental defects in these mice. Therefore, in order to determine the role of DOT1L during B cell responses, we generated novel mice in which *Dot1l*$^{f/f}$ mice were crossed with *Cd23*^{cre} mice. These mice deleted *Dot1l* specifically in mature B cells, leaving B cell development intact. As such, any phenotype in *Dot1l*$^{f/f}$*Cd23*$^{cre/+}$ mice should specifically be a consequence of the role of DOT1L in peripheral B cell differentiation and not due to the role of DOT1L observed during B cell development in the bone marrow. *Cd23*$^{cre/+}$ and *Dot1l*$^{f/f}$*Cd23*$^{cre/+}$ mice were immunized with the hapten (4-Hydroxy-3-nitrophenyl)-acetyl conjugated to Keyhole Limpet Hemocyanin (NP-KLH) precipitated on the adjuvant alum and GC B cell responses assessed at d7 and d28. At day 7, control mice generate a discernible NP^{+}CD95^{hi} GC B cell population (Figure 1A). In contrast, conditional deletion of DOT1L in B cells prohibited the formation of GC (Figure 1A). This was not due to delayed kinetics. Strikingly, GC B cell frequency (Figure 1B) and number (Figure 1C) were completely absent in *Dot1l*$^{f/f}$*Cd23*$^{cre/+}$ mice assessed during early (day 7) and late (day 28) phases of the response. While splenic morphology of B cell follicles appeared normal in *Dot1l*$^{f/f}$*Cd23*$^{cre/+}$ mice compared to *Cd23*$^{cre/+}$ controls (Figures 1D-1E), histological analyses showed a complete lack of PNA^{+} GC (Figure 1D) and IgG1^{+} cells

(Figure 1E). Therefore, DOT1L was essential for the formation of GC and $IgG1^+$ B cells during an immune response against alum-precipitated NP-KLH.

DOT1L is essential for the establishment of humoral immunity

The formation of immune memory is a critical outcome for an effective B cell response. Immune memory populations in the humoral arm of the immune system consist of memory B cells and long-lived plasma cells. In several gene-deficient models, the abrogation of GC responses is associated with an increase in early memory B cells (Good-Jacobson and Shlomchik, 2010). We therefore determined whether the absence of DOT1L affected the formation of immune memory subsets. *Cd23*$^{cre/+}$ and *Dot1l*$^{f/f}$*Cd23*$^{cre/+}$ mice were immunized with NP-KLH in alum and assessed at both day 7 and 28 post-immunization. Memory B cells, as defined by $NP^+IgG1^+CD38^+$, were completely absent in DOT1L-deficient mice (Figure 1F). At both days 7 and 28 post-immunization, memory B cell frequency (Figure 1G) and number (Figure 1H) were absent in *Dot1l*$^{f/f}$*Cd23*$^{cre/+}$ mice. Correspondingly, plasma cells in the bone marrow (Figure 1I) were also significantly decreased, with high-affinity antibody-secreting cells (ASCs) completely absent. As such, circulating NP-binding IgG1 antibody was significantly decreased (Figure 1J). Therefore, DOT1L was essential for the establishment of humoral memory following T-dependent immunization.

DOT1L is required for GC B cells in response to the Th1 cell-biased influenza infection

Inhibition of DOT1L in T helper (Th) cells was shown to result in an increase in both Th1 cells and IFNγ production by those cells in vitro (Scheer et al., 2019). B cells also have tailored functional responses to either Th1 cell-biased or Th2 cell-biased stimuli, and although transcription

factor expression is associated with dichotomous responses (Piovesan et al., 2017), it is not known whether epigenetic regulators are also important in specialized B cell function. Given the modulation of Th cell function by DOT1L, we used an influenza model to assess the role of DOT1L in an IFNγ-mediated B cell response and determine whether the role of DOT1L is generalizable across different types of responses in B cells. *Cd23*$^{cre/+}$ and *Dot1l*$^{f/f}$*Cd23*$^{cre/+}$ mice were infected with the H3N2 HKx31 influenza virus. B cell differentiation was assessed in the spleen and draining (mediastinal) lymph node 8 and 14 days post-infection. Concordant with the immunization results (Figure 1), DOT1L was required for B cells to mount an effective response to influenza. In the absence of DOT1L, there was a ≥5-fold decrease in splenic GC B cells (Figures 2A-2C) and a similar reduction of GC B cells in the mediastinal lymph node (Figures 2D-2E). Those GC B cells that remained were examined for isotype switching to IgG2c, and found to be ~2-fold decreased on a per GC B cell basis (Figure 2F). Finally, we excluded aberrant skewing of immunoglobulin isotypes by assessing Th2-associated IgG1 production in influenza-infected (Th1 cell-biased) mice, and conversely, Th1-associated IgG2c production in NP-KLH-immunized (Th2 cell-biased) mice. In both cases, antibody production of both isotypes was significantly reduced in the absence of DOT1L and thus there was no evidence of aberrant Th cell-biased responses these mice (Figures 2G and 2H, respectively). Therefore, DOT1L was essential for B cells to mount an effective GC reaction during either Th1 or Th2 cell-biased immune responses.

DOT1L is required for isotype-switched plasmablast formation in vivo

During the early phases of a T-dependent immunization, activated B cells either migrate back into the follicles and form GC B cells, or they can form foci of proliferating extrafollicular plasmablasts secreting low-affinity unswitched (IgM) and switched (IgG1) isotypes. As GC were unable to form

in the absence of DOT1L, we asked whether this was specific to GC B cell differentiation, or whether plasmablast differentiation was also abrogated in vivo. We first examined the frequency of formation of extrafollicular plasmablasts at day 7 post immunization. *Cd23*$^{cre/+}$ and *Dot1l*$^{f/f}$*Cd23*$^{cre/+}$ mice were immunized with NP-KLH in alum and splenic plasmablasts assessed as B220^{lo}CD138^{+} cells (Figure 3A). In the absence of DOT1L, there was a 3-fold reduction in plasmablasts (Figures 3B-3C). While a small population of plasmablasts remained in *Dot1l*$^{f/f}$*Cd23*$^{cre/+}$ mice, these cells had not switched to IgG1 (Figures 3D-3E). The formation of antigen-specific antibody-secreting plasmablasts, as well as circulating antibody, were also significantly diminished in the absence of DOT1L. NP-specific IgG1^{+} ASCs were absent from *Dot1l*$^{f/f}$*Cd23*$^{cre/+}$ mice (Figures 3F-3G). Accordingly, NP-binding IgG1 antibody was not detected in serum (Figure 3H). In contrast, there was little difference in NP-specific IgM ASCs (Figure 3I) and only a small reduction in NP-binding serum IgM (Figure 3J). While this was consistent with a defect in isotype switching, it may instead reflect the timing of DOT1L function. That is, the defect observed in DOT1L-deficient mice may have occurred after the formation of IgM^{+} plasmablasts in this model. Lastly, we also assessed the formation of plasmablasts during an influenza infection. Plasmablasts in both spleen (Figures 3K-3L) and mediastinal lymph node (Figures 3M- 3N), as well as serum IgG2c (Figure 3O), were significantly reduced. Together, these data demonstrated an absolute requirement for DOT1L for GC B cell and isotype-switched plasmablast formation in both Th2 and Th1 cell-biased responses.

DOT1L is required for mounting a B cell response independent of T cells or GCs

The results generated thus far revealed that DOT1L activity was important for establishing a GC and plasmablast response post-immunization with a T-dependent antigen. However, it remained

unclear if DOT1L was required for B cell responses that formed independently of T cell help or GCs, or possibly promoted the T-independent plasmablast pathway. To investigate these questions in more detail, *Cd23*$^{cre/+}$ and *Dot1l*$^{f/f}$*Cd23*$^{cre/+}$ mice were immunized with NP-Ficoll in PBS, we utilized a type 2 T-independent antigen and B cell differentiation assessed 5 days later. Both antigen-specific IgM^{+} (Figure 3P) and IgG3^{+} ASCs (Figures 3Q) were significantly reduced in the absence of DOT1L. Accordingly, circulating NP-binding IgM (Figure 3R) and IgG3 (Figure 3S) antibodies were both significantly reduced. Interestingly, there was a stronger defect in IgM in the T-independent response (Figure 3R) compared to the T-dependent response (Figure 3J). Nevertheless, these data demonstrate that DOT1L is required for effective B cell differentiation into ASCs and antibody production in both T-dependent and T-independent responses.

DOT1L regulates expression of genes required for effective B cell responses in vivo

The next series of experiments were undertaken to delineate how DOT1L regulates B cell fate. Histone modifiers have been linked with cell cycle regulation of B cells (Beguelin et al., 2017; Caganova et al., 2013). Given the absence of B cell responses across multiple immunization and infection models, we utilized two separate approaches to determine whether DOT1L-deficient B cells were unable to be activated, and/or were prone to undergo apoptosis. In the first, we compared cell trace violet (CTV)-labeled B cells isolated from *Cd23*$^{cre/+}$ and *Dot1l*$^{f/f}$*Cd23*$^{cre/+}$ mice stimulated *in vitro* with CD40L, IL-4 and IL-5. In the second, we incubated stimulated CTV-labeled wild-type B cells with a small molecule inhibitor to DOT1L (Scheer et al., 2019). In both cases, proliferation was not significantly affected in the absence of DOT1L and nor was cell death (data not shown). Thus, humoral responses were not prematurely aborted due to an intrinsic lack of cell proliferation or increased cell death in DOT1L-deficient B cells.

We next confirmed the target histone modification regulated by DOT1L in B cells. Specifically, we determined whether conditional deletion of DOT1L would result in a reduction of global H3K79me2 in B cell subsets (Figure S2A). As a control, we also tested polycomb repressive complex 2 (PRC2)-mediated H3K27me3, which has also been shown to be an important regulator of B cell biology (Beguelin et al., 2013; Caganova et al., 2013; Guo et al., 2018; Su et al., 2003). Splenic IgD^+ and IgD^- B cells were sort-purified from immunized *Cd23*$^{cre/+}$ and *Dot1l*$^{f/f}$*Cd23*$^{cre/+}$ mice, together with *Eed*$^{f/f}$*Cd23*$^{cre/+}$ mice as controls for PRC2 function (Figure S2A; EED is the scaffolding protein required for PRC2 assembly). As expected, in the absence of DOT1L, there was a global decrease in H3K79me2 in B cell subsets, but not in the absence of EED (Figure S2B-S2C). Conversely, global H3K27me3 was reduced in B cells in the absence of EED, but not in the absence of DOT1L (Figures S2D-S2E). Thus, these results confirmed that DOT1L specifically mediates H3K79 methylation in B cells.

This lead to us to hypothesize that DOT1L-mediated H3K79 methylation regulated unique transcriptional programs following B cell activation, which we assessed by RNA-sequencing. $CD19^+IgD^+$ naïve B cells and $CD19^+IgD^-$ B cells were sort-purified from NP-KLH in alum-immunized mice, the latter population being enriched in activated B cells during an immune response. To enrich for the immediate gene regulatory events, without the compounded impact of the absence of GC and early memory B cell populations, we isolated B cell subsets 4 days post-immunization, a time at which there was little difference in the frequency of antigen-specific B cells in DOT1L-deficient compared to DOT1L-sufficient mice (data not shown). As expected, the greatest differences were observed between $CD19^+IgD^+$ (naïve) and $CD19^+IgD^-$ (activated) B

cells, and then between control and DOT1L-deficient cells (Figure 4A). Of note, the majority of genes differentially expressed were upregulated in DOT1L-deficient $CD19^{+}IgD^{+}$ naïve B cells compared to control naïve B cells, with only 5 genes downregulated (Figures 4B-4C). In contrast, 30 genes were downregulated in DOT1L-deficient $CD19^{+}IgD^{-}$ B cells compared to controls (Figures 4D-4E), correlating to the association of H3K79me2 with actively transcribed genes during cell differentiation (Steger et al., 2008). There were 37 genes that overlapped between datasets (Figure S3A). Of these common genes, the vast majority (89%) were upregulated in the absence of DOT1L, with downregulated genes almost solely restricted to $CD19^{+}IgD^{-}$ B cells (Figures S3B, S3C and S3D, respectively).

In other cell types, DOT1L function has been linked with inhibiting inappropriate differentiation (Wong et al., 2015). Thus, we interrogated whether the expression of transcription factors that regulate differentiation steps in B cells, such as *Bcl6* and *IRF4* (Dent et al., 1997; Klein et al., 2006; Willis et al., 2014), was dysregulated. However, there was no observable difference in expression of these transcription factors (data not shown). Notably, *Aicda,* the gene encoding activation-induced cytidine deaminase (AID), was downregulated in the absence of DOT1L. AID is essential for class-switch recombination, and expression of AID is observed in pre-GC B cells early during a B cell response (Cooper and Good-Jacobson, 2019; Roco et al., 2019). Downregulation of *Aicda* in DOT1L-deficient activated B cells correlated with the decrease in isotype switching observed in all *in vivo* models (Figures 1-3).

Multiple genes associated with B cell activation and migration, such as *Ackr2, Ackr4, GCsam, S1pr2* and *Tnfrsf17,* were upregulated in B cells from $Cd23^{cre/+}$ upon activation, compared to naïve

B cells, but were not expressed in either DOT1L-deficient subsets (Figures 4E). Chemokine receptors expressed on B cells regulate their ability to migrate in response to chemokine gradients present in the microenvironment (Lu and Cyster, 2019). The atypical chemokine receptors Ackr2 and Ackr4 has been linked to regulation of B cell migration (Hansell et al., 2011; Kara et al., 2018). While the role of Ackr2 in GC responses has not yet been studied, Ackr4 has recently been identified as a negative regulator of B cell responses with enforced expression of Ackr4 reducing B cell migration towards CCL21, a CCR7 ligand (Kara et al., 2018). Correspondingly, DOT1L-deficient cells, which had a reduction in *Ackr4*, had an increased ability to migrate to CCL21 (Figure S3E). Furthermore, S1PR2 (the G protein-coupled sphingosine-1-phosphate receptor encoded by *S1pr2*) is critical for B cell confinement in the GC (Green and Cyster, 2012). While we did not observe in increase in GCs observed in Ackr4-deficient (Kara et al., 2018) and S1PR2-deficient (Green and Cyster, 2012) mice, we hypothesized that disruption of the expression of multiple genes associated with early activation and migratory events in DOT1L-deficient B cells may result in early defective humoral responses in vivo.

DOT1L regulates localization of activated B cells during a humoral response

During the first 3-4 days of an immune response, B cells migrate to the T:B border and the interfollicular zone before moving back into the follicle to establish GCs (Chan et al., 2009; Kerfoot et al., 2011; Kitano et al., 2011). To gain further insight into the networks of genes regulated by DOT1L during early B cell responses, Ingenuity Pathway Analysis (IPA) was performed. Notably, cellular movement, cell signalling and DNA replication and repair as the top three functions identified by IPA as being dysregulated in the absence of DO1L (Figure 5A). Further analysis revealed networks of molecules involved in cell migration (Figure 5B) and B cell

responses (Figure S3F). To investigate the effect of changes in these molecules, we immunized mice and assessed localization of cells in vivo 4 days post-immunization. In accordance with transcriptomic data, DOT1L-deficiency resulted in altered positioning of B cells within the spleen at the critical time juncture of nascent GC formation in vivo. In *Cd23*$^{cre/+}$ mice, B cell lymphoma-6 (BCL6)$^{+}$ B and T cells were observed in the follicle in nascent GC (Figure 5C; orange arrows), consistent with previous studies (Kerfoot et al., 2011; Kitano et al., 2011). In DOT1L-deficient mice, BCL6^{+} cells were detectable, confirming that upregulation of BCL6 in the early stages of the response could occur in *Dot1l*$^{f/f}$*Cd23*$^{cre/+}$ mice (Figure 5C). Yet in contrast to *Cd23*$^{cre/+}$ mice, DOT1L-deficient BCL6^{+} cells did not cluster together in the follicle. Instead, BCL6^{+} cells in *Dot1l*$^{f/f}$*Cd23*$^{cre/+}$ mice were observed to be located mainly outside the B220^{+} follicles (Figure 5C; white arrows). Specifically, BCL6^{+} cells were located in the outer edge of the follicle, potentially in the marginal zone, as well as in extrafollicular areas (Figures 5C), with quantitation revealing a >3-fold increase in BCL6^{+} cells positioned in the outer edge of the follicle in *Dot1l*$^{f/f}$*Cd23*$^{cre/+}$ mice compared to *Cd23*$^{cre/+}$ mice (Figure 5D). Additionally, more B220^{+} cells were observed to penetrate into the T cell zone in the absence of DOT1L (Figure 5C). Thus, dysregulation of a network of genes involved in cellular migration in *Dot1l*$^{f/f}$*Cd23*$^{cre/+}$ mice correlated with altered localization in the spleen during the initial stages of an immune response. Taken together, this study establishes DOT1L as a pivotal regulator of B cell development, antigen-driven B cell migration, differentiation and the establishment of long-lived humoral immune memory.

Elucidation of the critical histone modifiers that regulate B cell fate and function has significant implications for translational studies. In particular, dissecting the role of DOT1L in cellular biology is vital for understanding the biological effects of clinical intervention with DOT1L

inhibitors. A DOT1L small molecule inhibitor is currently in clinical trials for the treatment of *MLLr* leukemias (Stein and Tallman, 2015). Our results suggest that sustained inhibition of DOT1L could have an impact on B cell progenitors and the ability of the humoral system to respond to infection. Further, the critical role of DOT1L in multiple stages of B cell biology may indicate that DOT1L could be an important target for other B cell-derived cancers. For example, DOT1L was identified in a screen of patients with diffuse large B cell lymphoma (Szablewski et al., 2018). This raises the possibility that targeting DOT1L in GC B cell-derived lymphomas may be a potential, but as yet unexplored, novel therapeutic option.

In summary, we have identified DOT1L as a critical and central regulator of B cell biology. Here, we demonstrate for the first time that appropriate B cell development, as well as migration and ultimately differentiation during immune responses, requires DOT1L function. This work opens up new avenues of investigation in both understanding the fundamental molecular underpinnings of B cell responses and whether small molecule inhibitors targeting DOT1L may be effective in abrogating B cell-driven diseases.

ACKNOWLEDGEMENTS

We thank Mireille Lahoud and David Tarlinton for critical reading of this manuscript; members of the Good-Jacobson and Zaph labs, Monash Micromon and Bioinformatics Platforms for technical assistance. KLG-J is a Bellberry-Viertel Senior Medical Research Fellow and was supported by a National Health and Medical Research Council (NHMRC) Career Development Fellowship. ADiP was supported by an American Association of Immunologists Careers in Immunology Fellowship. This work was supported by a NHMRC project grant to JRG and KLG-J (GNT1137989). JRG was supported by a Walter and Eliza Hall Institute Centenary Fellowship sponsored by CSL. LK was supported by a Monash University Research Training Program Scholarship. LD was supported by a University of Melbourne research scholarship. CZ was funded by NHMRC Project grants GNT1104433 and GNT1104466. CZ is a veski Innovation Fellow.

Address correspondence to:

Kim Good-Jacobson

Email: kim.jacobson@monash.edu

AUTHOR CONTRIBUTIONS

KLG-J designed the research; LK, ADiP and LD performed research; JRG performed research and provided intellectual input; SS and CZ provided reagents, mice and intellectual input; and KLG-J wrote the manuscript.

DECLARATION OF INTERESTS

The authors declare no competing interests.

FIGURE LEGENDS

Figure 1: Dot1l deletion results in ablation of GCs and inability to form humoral memory.

(A) Flow cytometric representative plot of GC B cells in *Cd23*$^{Cre/+}$ and *Dot1l*$^{f/f}$*Cd23*$^{Cre/+}$ mice 7 days post-immunization with NP-KLH precipitated in alum. (B) *Cd23*$^{Cre/+}$ (black bars or closed squares) and *Dot1l*$^{f/f}$*Cd23*$^{Cre/+}$ (white bars or open circles) mice were immunized with NP-KLH precipitated in alum and assessed at days 7 and 28 post-immunization for (B) frequency and (C) number of splenic CD19^{+}IgD^{-}NP^{+}CD95^{+} cells. (D) Representative images from histological analyses day 7 post-immunization: B220 (red) and PNA (blue). Scale bar = 100μm. (E) Representative images from histological analyses day 7 post-immunization: B220 (red) and IgG1 (blue). Scale bar = 100μm. (F) Flow cytometric representative plot of NP^{+}IgG1^{+}CD38^{+} memory B cells. (G) Frequency and (H) total number of memory B cells in the spleen. (I) ELISpot analysis of IgG1^{+}NP^{+} ASCs in the bone marrow at day 28 post-immunization. (J) ELISA analysis of NP^{+}IgG1 serum antibody 28 days post-immunization. Results are compiled from experiments performed at two separate time points: day 7 (*Cd23*$^{Cre/+}$ (n=6) and *Dot1l*$^{f/f}$*Cd23*$^{Cre/+}$ (n=6) mice; combined from two independent experiments) and day 28 (n=7 per genotype; combined from two independent experiments) post-immunization with NP-KLH in alum. ** $P < 0.01$; *** $P < 0.001$.

Figure 2: DOT1L is necessary to produce an efficient humoral immune response to the HKx31 influenza virus.

(A) *Cd23*$^{Cre/+}$ and *Dot1l*$^{f/f}$*Cd23*$^{Cre/+}$ mice were intranasally infected with HKx31 and culled for analysis 8 days and 14 days post-infection. Flow cytometric representative plot of CD95^{+}CD38^{lo} splenic GC B cells. (B-C) Frequency (B) and (C) number of CD95^{+}CD38^{lo} GC B cells in the spleen. (D-E) Frequency (D) and (E) number of CD95^{+}CD38^{lo} GC B cells in the mediastinal lymph

node. (F) Frequency of splenic and mediastinal lymph nodes GC B cells that have switched to IgG2c. n=6 per genotype, combined from two independent experiments per time point. * $P < 0.05$; ** $P < 0.01$. (G) ELISA analysis of IgG1 serum antibody from *Cd23*$^{Cre/+}$ (closed squares) and *Dot1l*$^{f/f}$ *Cd23*$^{Cre/+}$ mice (open circles) infected with influenza. (H) ELISA analysis of NP^{+}IgG2c serum antibody from *Cd23*$^{Cre/+}$ and *Dot1l*$^{f/f}$ *Cd23*$^{Cre/+}$ mice immunized with NP-KLH in alum. ** $P < 0.01$.

Figure 3: DOT1L plays a key role in the formation and class-switching of early splenic plasma cells produced in response to TD antigens.

(A) Flow cytometry representative plot of B220^{lo}CD138^{+} cells in the presence or absence of Dot1L 7 days post-immunization with NP-KLH in alum. (B-C) Frequency (B) and (C) number of B220^{lo}CD138^{+} cells in *Cd23*$^{Cre/+}$ (black bars) and *Dot1l*$^{f/f}$*Cd23*$^{Cre/+}$ mice (light grey bars). (D) Flow representative plot and (E) frequency of IgG1^{+} cells within the B220^{lo}CD138^{+} population. (F-G) ELISpot analysis of NP^{+} IgG1^{+} ASCs in the spleen at day 7 post-immunization. (H) Serum NP^{+}IgG1 antibody at day 7 post-immunization. (I) ELISpot analysis of NP^{+}IgM^{+} ASCs in the spleen at day 7 post-immunization. (J) Serum NP^{+}IgM antibody at day 7 post-immunization. Results are compiled from experiments performed at two separate time points: day 7 (*Cd23*$^{Cre/+}$ (n=6) and *Dot1l*$^{f/f}$*Cd23*$^{Cre/+}$ (n=6) mice; combined from two independent experiments) and day 28 (n=7 per genotype; combined from two independent experiments) post-immunization with NP-KLH in alum. (K-N) *Cd23*$^{Cre/+}$ and *Dot1l*$^{f/f}$*Cd23*$^{Cre/+}$ mice were infected with HKx31 influenza virus and assessed 8 and 14 days post-infection for (K) frequency and (L) number of B220^{lo}CD138^{+} cells in the spleen, and (M) frequency and (N) number of B220^{lo}CD138^{+} cells in the mediastinal lymph node. (O) Total serum IgG2c at day 14 post-infection. n=6 per genotype,

combined from two independent experiments per time point. * $P < 0.05$; ** $P < 0.01$; **** $P < 0.0001$. (P) ELISpot analysis of splenic NP^+IgM^+ ASCs 5 days post-immunization with NP-Ficoll in *Cd23*$^{Cre/+}$ (black bars or closed squares) and *Dot1l*$^{f/f}$*Cd23*$^{Cre/+}$ mice (light grey bars or open circles). (Q) Splenic NP^+IgG3^+ ASCs. (R) NP^+ IgM and (S) NP^+ IgG3 serum antibody. n=6 per genotype, combined from two independent experiments per time point. * $P < 0.05$.

Figure 4: DOT1L regulates expression of genes required for effective B cell responses in vivo. (A-D) RNA-sequencing data: each sample is an independent sample obtained from either $CD19^+IgD^+$ or $CD19^+IgD^-$ B cells sort-purified from either *Dot1l*$^{f/f}$*Cd23*$^{Cre/+}$ or *Cd23*$^{Cre/+}$ mice 4 days post-immunization with NP-KLH in alum. (A) Multidimensional scaling plot of each sample assessed by RNA-sequencing. (B) MA plot for $CD19^+IgD^+$ samples. Shown is the average expression vs log fold change of *Dot1l*$^{f/f}$*Cd23*$^{Cre/+}$ samples compared to *Cd23*$^{Cre/+}$ samples. A FDR cutoff of 0.01 and absolute log fold change of 1 was applied to the samples. (C) Heatmap of RNA-sequencing data (Table S1); each column is an independent sample obtained from sort-purified $CD19^+IgD^+$ B cells from either *Dot1l*$^{f/f}$*Cd23*$^{Cre/+}$ or *Cd23*$^{Cre/+}$ mice immunized with NP-KLH in alum. (D) MA plot for $CD19^+IgD^-$ samples. Shown is the average expression vs log fold change of *Dot1l*$^{f/f}$*Cd23*$^{Cre/+}$ samples compared to *Cd23*$^{Cre/+}$ samples. A FDR cutoff of 0.01 and absolute log fold change of 1 was applied to the samples. (E) Heatmap of RNAseq data (Table S2); each column is an independent sample obtained from sort-purified $CD19^+IgD^-$ B cells from either *Dot1l*$^{f/f}$*Cd23*$^{Cre/+}$ or *Cd23*$^{Cre/+}$ mice immunized with NP-KLH in alum. (F) Plots showing count per million for individual genes. Colours as per multidimensional scaling plot shown in (A).

Figure 5: DOT1L regulates localization of activated B cells during a humoral response

(A) IPA was used for the biological functions and pathway analysis of differentially expressed genes in $CD19^{+}IgD^{-}$ samples. Summary of top molecular and cellular function regulated by Dot1L. (B) Prediction analysis of potential diseases and functions from sets of identified differentially expressed genes in $CD19^{+}IgD^{-}$ samples. Annotation of altered genes involved in cell movement of leukocytes. The different colours indicate the expression level of the genes (red indicating up-regulated genes and green indicating down-regulated genes) or the predicted activity of the identified gene in the activation (blue) or inhibition (orange) of the specified function. The dashed arrows indicate the indirect relationship of the annotated gene to the altered function. (C) Representative images from histological analyses day 4 post-immunization: B220 (yellow), CD4/CD8 (magenta) and BCL6 (blue). Scale bar = 100μm. (D) Quantitation of $BCL6^{+}$ cells in the outer edge of follicles. * $P < 0.05$.

MATERIALS AND METHODS

Mice, immunizations and purification of cells

Mb1-Cre (Pelanda et al., 2002), *Eed*$^{f/f}$ (Xie et al., 2014) and *Cd23*-Cre (Kwon et al., 2008) were provided by Michael Reth, Stuart Orkin and Meinrad Busslinger, respectively. To create *Dot1l*$^{f/f}$ mice, we derived mice from DOT1L targeted ES cells (Dot1ltm1a(KOMP)Wtsi) from UCDavis KOMP Repository and crossed them with FLP mice (Monash University). Subsequently, *Dot1l*$^{f/f}$ mice were crossed with *Mb1-Cre* or *Cd23-Cre* (all on C57BL/6 background). Animal procedures were approved by Monash University Animal Ethics Committee and all mice were maintained at the Monash Animal Research Platform. Mice at least 6 weeks of age and of either gender were used in this study. Mice were humanely euthanized by hypercapnea. *T-dependent immunization model:* (4-Hydroxy-3-nitrophenyl)-acetyl (NP) hapten was conjugated to Keyhole Limpet Hemocyanin (NP_{13}KLH), precipitated on 10% Alum and diluted in sterile PBS to a final concentration of 100µg/100µl. *T-independent immunization model:* NP_{55}Ficoll was diluted in sterile PBS to a final concentration of 40µg/100µl. *Influenza infections:* Mice were inoculated with 250p.f.u. of HKx31 (H3N2) influenza virus, generously provided by Gabrielle Belz and Stephen Turner, as previously described (Belz et al., 2000; Flynn et al., 1998). *Anasthesia*: Isofluorane (2.5%) was used to lightly anesthetize mice for intranasal infections. Mice were monitored to ensure stabilization of breathing and were warmed by a lamp to alleviate suffering if necessary.

Flow cytometry

Single cells were resuspended in PBS 2% FCS and stained for flow cytometric analysis as previously described (Cooper et al., 2018). Briefly, 5 x 10^6 cells were resuspended in 50µl of FVS fixable viability stain, diluted 1:1000 in PBS 2% FCS and incubated for 15 minutes at room

temperature in the dark. Samples were then washed with PBS 2% FCS, and then resuspended in 50µl of indicated antibodies (Table S3) and incubated at 4°C for 20 minutes. FcγRII/III (24G2; supernatant) and normal rat serum (Sigma-Aldrich) was used to block non-specific binding. Cells were then washed and resuspended in PBS 2% FCS and data acquired on a BD Fortessa or LSRIIa and subsequently analyzed using FlowJo (Tree Star). *Sort-purification*: cells were stained with antibodies and purified by FACS Influx (BD), with purity >98%.

ELISPOT

ASCs of the IgG1, IgG3 and IgM isotype were analyzed by ELISPOT. Multiscreen HA plates (Millipore) were coated overnight at 4°C with NP_{12}BSA for the quantification of NP-specific $IgG1^+$ and $IgG3^+$ ASCs. An NP_9BSA coat was used to analyze total NP^+IgM^+ ASCs while NP_1BSA was used to measure high-affinity $IgG1^+$ ASCs. Plates were blocked with PBS 1%BSA for 1 hour, washed with PBS, and loaded with samples prepared in RPMI 5%FCS, 50µM 2-Mercaptoethanol and 2mM Glutamine before an overnight incubation at 37°C. Plates were washed with PBS-Tween and distilled water and subsequently incubated for 1 hour at 37°C with secondary antibody (IgG1, IgG3 or IgM) conjugated to alkaline-phosphatase (Southern Biotech) for one hour. Plates were washed, as before, and developed with the BCiP®/NBT reaction (Sigma-Aldrich).

ELISA

Serum samples from mice immunized with NP-KLH or NP-Ficoll were assessed by coating 96-well high binding plates (Sarstedt), overnight at 4°C, with 5µg/µl NP_9BSA for IgM^+ antibodies or NP_{12}BSA for all other isotypes. Serum samples from naïve mice or influenza-infected mice were analyzed by coating plates with the appropriate isotype-specific capture antibody (Southern

Biotech; Table S3). Plates were blocked, the following day, with PBS 1%BSA for 1 hour, washed with PBS-Tween and distilled water and then loaded with serially-diluted serum samples before a 4-hour incubation at 37°C. Plates were washed again with PBS-Tween and distilled water and then incubated for 1 hour at 37°C with the appropriate anti-mouse secondary antibody conjugated to horseradish peroxidase (Southern Biotech; Table S3). Plates were washed and developed with OPD-substrate solution (Sigma-Aldrich). Serum was serially diluted in block and the optical density values for each sample are shown as a non-linear regression (sigmoidal curve fit).

Immunohistochemistry

Spleens from mice immunized with NP-KLH were extracted, 7 days post-immunization, and frozen in OCT (Tissue-Tek). 7μm sections were cut using a microtome (Leica) at -20°C and fixed with acetone. Staining was performed using described antibodies (Table S3). Slides were viewed under 4X and 10X magnification using an Olympus CKX41 microscope and images were captured with a mounted Nikon DP-12 camera. Raw images were taken using the Nikon NIS-Element software platform while the processing program, ImageJ, was used to add 100μm scale bars to each image.

Immunofluorescence

Spleens were either directly embedded in OCT compound (Tissue-Tek), or first fixed in 4% paraformaldehyde and immersed in 30% sucrose before being embedded in OCT compound (Tissue-Tek). Tissues were cut via microtome (Leica) into 12μm sections and mounted on Superfrost Plus slides. Sections were fixed with cold acetone (Sigma) and stained as previously described (Rankin et al., 2013) and using indicated antibodies (Table S3). Images were acquired

using a LSM780 confocal microscope (Carl Zeiss MicroImaging). The acquisition software was Zen Black 2012.

Chemotaxis assay

B cells were isolated using negative B cell isolation kit (Stem Cell) and resuspended in 0.5% FBS, RPMI 1640 at $5x10^5$cells per well. 100µl/well were added to the upper chamber of transwell plates and transmigrated across 3µm transwell filters (Corning Costar Corp, NY, USA) for 3 hours. Chemotaxis agent CCL21 (Peprotech, NJ, USA) diluted in 0.5% FBS, RPMI 1640 was added to the bottom chamber at indicated concentrations. Post migration, cells were collected, stained for surface markers (Table S3) and analysed and enumerated by flow cytometry.

RNA-sequencing and bioinformatics analysis

Sort-purified cell subsets were centrifuged, lysed in RLP Buffer (QIAGEN) and passed through a gDNA eliminator spin column (QIAGEN) to remove genomic DNA. The flow-through was passed through a silica-membrane designed to capture RNA (QIAGEN), which was then washed and dried following the manufacturer's recommendations (QIAGEN RNeasy Plus Micro Kit), and eluted in 14µl of RNase-free H2O. The 8 RNA samples were prepped using the Illumina Truseq stranded mRNA sample preparation kit with the input RNA of 100ng and sequence using Illumina Nextseq 500 Single End 75 cycles high output version2 cartridge. Raw fastq files were analyzed using the RNAsik pipeline (Tsyganov et al., 2018) using STAR aligner (Dobin et al., 2013) with the GRCm38.p4 Ensembl reference. Reads were quantified using featureCounts (Liao et al., 2014) producing the raw genes count matrix and various quality control metrics. Raw counts were then analyzed with Degust (Powell, 2015), a web tool which performs differential expression analysis

using limma voom normalisation (Law et al., 2014), producing counts per million (CPM) library size normalisation and trimmed mean of M values normalisation (Robinson and Oshlack, 2010) for RNA composition normalisation. Degust (Powell, 2015) also provides quality plots including classical multidimensional scaling and MA plots. Data is shown with only protein coding genes and with immunoglobulin genes removed. IPA (QIAGEN) was used for the biological functions and pathway analysis of differentially expressed genes.

Histone Extractions and Western Blotting

$1x10^6$ cells were isolated per sample using fluorescence-activated cell sorting and lysed, overnight at 4^oC, in 0.2M HCl. Cell debris was pelleted and the recovered supernatant was treated at 95^oC, for 5 min, in SDS-PAGE loading buffer (250mM Tris- HCl pH 6.8, 10% SDS, 50% Glycerol, 0.05% bromophenol blue, 5% 2-mercaptoethanol). Samples were resolved on a 12% SDS-PAGE and analyzed by western blot using anti-H3 (Abcam ab1791), anti-H3K27me3 (Abcam ab6002) and anti-H3K79me2 (Abcam ab3594) antibodies. Blots were further stained with Horseradish Peroxidase- conjugated goat anti-mouse (Southern Biotech) or anti-rabbit IgG (H + L) antibodies (Biorad), developed with Clarity Western ECL Substrate (Biorad) and scanned on the ChemiDoc™ Touch Imaging System (Biorad).

Statistics

The Mann-Whitney nonparametric, two-tailed test was used for statistical analyses of all data, with the exception of western blot data, using GraphPad Prism software. Paired t-test was used for statistical analyses of western blot data, using GraphPad Prism software. All data is presented as the mean +/- the standard error of the mean. n = the number of individual mice assessed.

The accession number for the RNA-seq data reported in this paper is GEO: https://www.ncbi.nlm.nih.gov/geo/query/acc.cgi?acc=GSE138401

SUPPLEMENTAL INFORMATION

Figure S1: Conditional Dot1l deletion disrupts B cell development.

(A) Schematic of conditional deletion of *Dot1l* in the B cell lineage. (B) Representative image of spleens isolated from $Mb1^{Cre/+}$ (left) and $Dot1l^{f/f}$ $Mb1^{Cre/+}$ (right) mice. (C) Spleen weight of naïve, adult $Mb1^{Cre/+}$ (black bars) and $Dot1l^{f/f}Mb1^{Cre/+}$ mice (light grey bars). Results are combined from 2 independent experiments. (D) Flow cytometric analyses of $CD19^{+}$ B cells in the spleen of naïve, adult $Mb1^{Cre/+}$ (black bars), $Dot1l^{fl+}$ $Mb1^{Cre/+}$ (grey bars) and $Dot1l^{f/f}Mb1^{Cre/+}$ mice (light grey bars). (E) Representative images from histological analyses of spleens from naïve mice: MOMA-1 (yellow) and B220 (magenta). Scale bar = 100μm. (F-I) Frequency and number of (F-G) marginal zone B cells and (H-I) follicular B cells in the spleen. (J-O) Different antibody isotypes from the serum of $Mb1^{Cre/+}$ (black squares) and $Dot1l^{f/+}$ and $Dot1l^{f/f}$ $Mb1^{Cre/+}$ mice (white circles) were compared by ELISA analysis: (J) total IgM, (K) total IgG1, (L) total IgG2c, (M) total IgG2b, (N) total IgG3 and (O) total IgA serum levels for each mouse group (n=6). Sigmoidal curve fit of serially diluted samples. (P-Q) Flow cytometric analyses of B cell populations in the bone marrow of naïve, adult $Mb1^{Cre/+}$ (black bars), $Dot1l^{fl+}$ $Mb1^{Cre/+}$ (grey bars) and $Dot1l^{f/f}Mb1^{Cre/+}$ mice (light grey bars). (P) $B220^{+}$ populations, (Q) Pro B cell ($B220^{lo}CD24^{+}BP1^{-}CD43^{+}IgM^{-}$), Pre B cell ($B220^{lo}CD24^{+}BP1^{+}CD43^{-}IgM^{-}IgD^{-}$), Immature B cell ($B220^{+}CD24^{+}CD43^{-}IgM^{lo}IgD^{-}$), Transitional B cell ($B220^{+}CD24^{+}CD43^{-}IgM^{hi}IgD^{-}$), Early Mature B cell ($B220^{+}CD24^{+}CD43^{-}IgM^{hi}IgD^{+}$) and Late Mature B cell ($B220^{+}CD24^{+}CD43^{-}IgM^{lo}IgD^{+}$) populations in the bone marrow. $Mb1^{Cre/+}$ (n=8), $Dot1l^{f/+}Mb1^{Cre/+}$ (n=5) and $Dot1l^{f/f}Mb1^{Cre/+}$ (n=7) mice. Results are combined from four independent experiments. * $P < 0.05$; ** $P < 0.01$; *** $P < 0.001$.

Figure S2: Regulation of global histone modifications in B cells by DOT1L and PRC2.

(A) Schematic of assessment of H3K79me2 and H3K27me3: mice were immunized with NP-KLH in alum and $CD19^{+}IgD^{+}$ and $CD19^{+}IgD^{-}$ B cell subsets sort-purified post-immunization. (B) Assessment of global H3K79me2 in sort-purified B cell subsets. (C) Quantitation of global H3K79me2. (D) Assessment of global H3K27me3 in sort-purified B cell subsets. (E) Quantitation of global H3K27me3. Blot images are cropped to show area around either H3K27me3 or H3K79me2 bands. No lanes were removed. n=3 per group, combined from three independent experiments. * $P < 0.05$; ** $P < 0.01$.

Figure S3: Modulation of genes in the absence of DOT1L in mature B cell subsets.

(A) Venn Diagram of differential expressed genes was obtained using the Comparison Analysis tool in IPA software to compare different sets of naive and activated B cells. (B-D) Bar graphs of genes differentially expressed solely in the $CD19^{+}IgD^{+}$ B cell population (B), common differential genes modulated in both B cell subsets (C), those solely in the $CD19^{+}IgD^{-}$ B cell population (D). (E) Migration of $CD19^{+}IgD^{-}NP^{+}$ splenic B cells towards CCL21. B cells were isolated from either $Dot1l^{f/f}Cd23^{Cre/+}$ or $Cd23^{Cre/+}$ mice 4 days post-immunization with NP-KLH in alum. Error bars are mean +/- the standard error of the mean. (F) Prediction analysis of potential diseases and functions from sets of identified differentially expressed genes in $CD19^{+}IgD^{-}$ samples. Annotation of altered genes involved in the regulation of B cells numbers. The different colours indicate the expression level of the genes (red indicating up-regulated genes and green indicating down-regulated genes) or the predicted activity of the identified gene in the activation (blue) or inhibition

(orange) of the specified function. The dashed arrows indicate the indirect relationship of the annotated gene to the altered function.

Table S1: Differential gene expression in CD19^{+}IgD^{+} B cells.

Table S2: Differential gene expression in CD19^{+}IgD^{-} B cells.

Table S3: Antibodies and reagents.

REFERENCES

Alberghini, F., Petrocelli, V., Rahmat, M., and Casola, S. (2015). An epigenetic view of B-cell disorders. Immunol Cell Biol *93*, 253-260.

Arrowsmith, C.H., Bountra, C., Fish, P.V., Lee, K., and Schapira, M. (2012). Epigenetic protein families: a new frontier for drug discovery. Nat Rev Drug Discov *11*, 384-400.

Beguelin, W., Popovic, R., Teater, M., Jiang, Y., Bunting, K.L., Rosen, M., Shen, H., Yang, S.N., Wang, L., Ezponda, T.*, et al.* (2013). EZH2 is required for germinal center formation and somatic EZH2 mutations promote lymphoid transformation. Cancer cell *23*, 677-692.

Beguelin, W., Rivas, M.A., Calvo Fernandez, M.T., Teater, M., Purwada, A., Redmond, D., Shen, H., Challman, M.F., Elemento, O., Singh, A., and Melnick, A.M. (2017). EZH2 enables germinal centre formation through epigenetic silencing of CDKN1A and an Rb-E2F1 feedback loop. Nat Commun *8*, 877.

Belz, G.T., Xie, W., Altman, J.D., and Doherty, P.C. (2000). A previously unrecognized H-2D(b)-restricted peptide prominent in the primary influenza A virus-specific CD8(+) T-cell response is much less apparent following secondary challenge. Journal of virology *74*, 3486-3493.

Bernt, K.M., Zhu, N., Sinha, A.U., Vempati, S., Faber, J., Krivtsov, A.V., Feng, Z., Punt, N., Daigle, A., Bullinger, L.*, et al.* (2011). MLL-rearranged leukemia is dependent on aberrant H3K79 methylation by DOT1L. Cancer cell *20*, 66-78.

Caganova, M., Carrisi, C., Varano, G., Mainoldi, F., Zanardi, F., Germain, P.L., George, L., Alberghini, F., Ferrarini, L., Talukder, A.K.*, et al.* (2013). Germinal center dysregulation by histone methyltransferase EZH2 promotes lymphomagenesis. J Clin Invest *123*, 5009-5022.

Chan, T.D., Gatto, D., Wood, K., Camidge, T., Basten, A., and Brink, R. (2009). Antigen affinity controls rapid T-dependent antibody production by driving the expansion rather than the differentiation or extrafollicular migration of early plasmablasts. J Immunol *183*, 3139-3149.

Cooper, L., and Good-Jacobson, K.L. (2019). B Cells Hit a Class Ceiling in the Germinal Center. Immunity *51*, 206-208.

Cooper, L., Hailes, L., Sheikh, A., Zaph, C., Belz, G.T., Groom, J.R., and Good-Jacobson, K.L. (2018). Assessing the role of the T-box transcription factor Eomes in B cell differentiation during either Th1 or Th2 cell-biased responses. PLoS One *13*, e0208343.

Dent, A.L., Shaffer, A.L., Yu, X., Allman, D., and Staudt, L.M. (1997). Control of inflammation, cytokine expression, and germinal center formation by BCL-6. Science *276*, 589-592.

Dobin, A., Davis, C.A., Schlesinger, F., Drenkow, J., Zaleski, C., Jha, S., Batut, P., Chaisson, M., and Gingeras, T.R. (2013). STAR: ultrafast universal RNA-seq aligner. Bioinformatics *29*, 15-21.

Flynn, K.J., Belz, G.T., Altman, J.D., Ahmed, R., Woodland, D.L., and Doherty, P.C. (1998). Virus-specific CD8+ T cells in primary and secondary influenza pneumonia. Immunity *8*, 683-691.

Geng, H., Brennan, S., Milne, T.A., Chen, W.Y., Li, Y., Hurtz, C., Kweon, S.M., Zickl, L., Shojaee, S., Neuberg, D.*, et al.* (2012). Integrative epigenomic analysis identifies biomarkers and therapeutic targets in adult B-acute lymphoblastic leukemia. Cancer Discov *2*, 1004-1023.

Good-Jacobson, K.L. (2018). Strength in diversity: Phenotypic, functional, and molecular heterogeneity within the memory B cell repertoire. Immunol Rev *284*, 67-78.

Good-Jacobson, K.L. (2019). B cells turn on, tune in with LSD1. Nat Immunol *20*, 3-5.

Good-Jacobson, K.L., Chen, Y., Voss, A.K., Smyth, G.K., Thomas, T., and Tarlinton, D. (2014). Regulation of germinal center responses and B-cell memory by the chromatin modifier MOZ. Proc Natl Acad Sci U S A *111*, 9585-9590.

Good-Jacobson, K.L., and Shlomchik, M.J. (2010). Plasticity and heterogeneity in the generation of memory B cells and long-lived plasma cells: the influence of germinal center interactions and dynamics. J Immunol *185*, 3117-3125.

Green, J.A., and Cyster, J.G. (2012). S1PR2 links germinal center confinement and growth regulation. Immunol Rev *247*, 36-51.

Guo, M., Price, M.J., Patterson, D.G., Barwick, B.G., Haines, R.R., Kania, A.K., Bradley, J.E., Randall, T.D., Boss, J.M., and Scharer, C.D. (2018). EZH2 Represses the B Cell Transcriptional Program and Regulates Antibody-Secreting Cell Metabolism and Antibody Production. J Immunol *200*, 1039-1052.

Haines, R.R., Barwick, B.G., Scharer, C.D., Majumder, P., Randall, T.D., and Boss, J.M. (2018). The Histone Demethylase LSD1 Regulates B Cell Proliferation and Plasmablast Differentiation. J Immunol *201*, 2799-2811.

Hansell, C.A., Schiering, C., Kinstrie, R., Ford, L., Bordon, Y., McInnes, I.B., Goodyear, C.S., and Nibbs, R.J. (2011). Universal expression and dual function of the atypical chemokine receptor D6 on innate-like B cells in mice. Blood *117*, 5413-5424.

Hatzi, K., Geng, H., Doane, A.S., Meydan, C., LaRiviere, R., Cardenas, M., Duy, C., Shen, H., Vidal, M.N.C., Baslan, T.*, et al.* (2019). Histone demethylase LSD1 is required for germinal center formation and BCL6-driven lymphomagenesis. Nat Immunol *20*, 86-96.

Inaba, H., Greaves, M., and Mullighan, C.G. (2013). Acute lymphoblastic leukaemia. Lancet *381*, 1943-1955.

Kara, E.E., Bastow, C.R., McKenzie, D.R., Gregor, C.E., Fenix, K.A., Babb, R., Norton, T.S., Zotos, D., Rodda, L.B., Hermes, J.R.*, et al.* (2018). Atypical chemokine receptor 4 shapes activated B cell fate. J Exp Med *215*, 801-813.

Kerfoot, S.M., Yaari, G., Patel, J.R., Johnson, K.L., Gonzalez, D.G., Kleinstein, S.H., and Haberman, A.M. (2011). Germinal center B cell and T follicular helper cell development initiates in the interfollicular zone. Immunity *34*, 947-960.

Kitano, M., Moriyama, S., Ando, Y., Hikida, M., Mori, Y., Kurosaki, T., and Okada, T. (2011). Bcl6 protein expression shapes pre-germinal center B cell dynamics and follicular helper T cell heterogeneity. Immunity *34*, 961-972.

Klein, U., Casola, S., Cattoretti, G., Shen, Q., Lia, M., Mo, T., Ludwig, T., Rajewsky, K., and Dalla-Favera, R. (2006). Transcription factor IRF4 controls plasma cell differentiation and class-switch recombination. Nat Immunol *7*, 773-782.

Krivtsov, A.V., Feng, Z., Lemieux, M.E., Faber, J., Vempati, S., Sinha, A.U., Xia, X., Jesneck, J., Bracken, A.P., Silverman, L.B.*, et al.* (2008). H3K79 methylation profiles define murine and human MLL-AF4 leukemias. Cancer cell *14*, 355-368.

Kwon, K., Hutter, C., Sun, Q., Bilic, I., Cobaleda, C., Malin, S., and Busslinger, M. (2008). Instructive role of the transcription factor E2A in early B lymphopoiesis and germinal center B cell development. Immunity *28*, 751-762.

Law, C.W., Chen, Y., Shi, W., and Smyth, G.K. (2014). voom: Precision weights unlock linear model analysis tools for RNA-seq read counts. Genome Biol *15*, R29.

Liao, Y., Smyth, G.K., and Shi, W. (2014). featureCounts: an efficient general purpose program for assigning sequence reads to genomic features. Bioinformatics *30*, 923-930.

Lu, E., and Cyster, J.G. (2019). G-protein coupled receptors and ligands that organize humoral immune responses. Immunol Rev *289*, 158-172.

Milcarek, C., Albring, M., Langer, C., and Park, K.S. (2011). The eleven-nineteen lysine-rich leukemia gene (ELL2) influences the histone H3 protein modifications accompanying the shift to secretory immunoglobulin heavy chain mRNA production. J Biol Chem *286*, 33795-33803.

Okada, Y., Feng, Q., Lin, Y., Jiang, Q., Li, Y., Coffield, V.M., Su, L., Xu, G., and Zhang, Y. (2005). hDOT1L links histone methylation to leukemogenesis. Cell *121*, 167-178.

Pelanda, R., Hobeika, E., Kurokawa, T., Zhang, Y., Kuppig, S., and Reth, M. (2002). Cre recombinase-controlled expression of the mb-1 allele. Genesis *32*, 154-157.

Piovesan, D., Tempany, J., Di Pietro, A., Baas, I., Yiannis, C., O'Donnell, K., Chen, Y., Peperzak, V., Belz, G.T., Mackay, C.R.*, et al.* (2017). c-Myb Regulates the T-Bet-Dependent Differentiation Program in B Cells to Coordinate Antibody Responses. Cell reports *19*, 461-470.

Powell, D. (2015). Degust: interactive RNA-seq analysis.

Rankin, L.C., Groom, J.R., Chopin, M., Herold, M.J., Walker, J.A., Mielke, L.A., McKenzie, A.N., Carotta, S., Nutt, S.L., and Belz, G.T. (2013). The transcription factor T-bet is essential for the development of NKp46 innate lymphocytes via the Notch pathway. Nat Immunol.

Robinson, M.D., and Oshlack, A. (2010). A scaling normalization method for differential expression analysis of RNA-seq data. Genome Biol *11*, R25.

Roco, J.A., Mesin, L., Binder, S.C., Nefzger, C., Gonzalez-Figueroa, P., Canete, P.F., Ellyard, J., Shen, Q., Robert, P.A., Cappello, J.*, et al.* (2019). Class-Switch Recombination Occurs Infrequently in Germinal Centers. Immunity *51*, 337-350 e337.

Scheer, S., Ackloo, S., Medina, T.S., Schapira, M., Li, F., Ward, J.A., Lewis, A.M., Northrop, J.P., Richardson, P.L., Kaniskan, H.U.*, et al.* (2019). A chemical biology toolbox to study protein methyltransferases and epigenetic signaling. Nat Commun *10*, 19.

Steger, D.J., Lefterova, M.I., Ying, L., Stonestrom, A.J., Schupp, M., Zhuo, D., Vakoc, A.L., Kim, J.E., Chen, J., Lazar, M.A.*, et al.* (2008). DOT1L/KMT4 recruitment and H3K79 methylation are ubiquitously coupled with gene transcription in mammalian cells. Mol Cell Biol *28*, 2825-2839.

Stein, E.M., and Tallman, M.S. (2015). Mixed lineage rearranged leukaemia: pathogenesis and targeting DOT1L. Curr Opin Hematol *22*, 92-96.

Strahl, B.D., and Allis, C.D. (2000). The language of covalent histone modifications. Nature *403*, 41-45.

Su, I.H., Basavaraj, A., Krutchinsky, A.N., Hobert, O., Ullrich, A., Chait, B.T., and Tarakhovsky, A. (2003). Ezh2 controls B cell development through histone H3 methylation and Igh rearrangement. Nat Immunol *4*, 124-131.

Szablewski, V., Bret, C., Kassambara, A., Devin, J., Cartron, G., Costes-Martineau, V., and Moreaux, J. (2018). An epigenetic regulator-related score (EpiScore) predicts survival in patients with diffuse large B cell lymphoma and identifies patients who may benefit from epigenetic therapy. Oncotarget *9*, 19079-19099.

Tsyganov, K., Perry, A.J., Archer, S.K., and Powell, D. (2018). RNAsik: A Pipeline for Complete and Reproducible RNA-seq Analysis That Runs Anywhere with Speed and Ease. Journal of Open Source Software *3*, 583.

Willis, S.N., Good-Jacobson, K.L., Curtis, J., Light, A., Tellier, J., Shi, W., Smyth, G.K., Tarlinton, D.M., Belz, G.T., Corcoran, L.M.*, et al.* (2014). Transcription factor IRF4 regulates germinal center cell formation through a B cell-intrinsic mechanism. J Immunol *192*, 3200-3206.

Wong, M., Polly, P., and Liu, T. (2015). The histone methyltransferase DOT1L: regulatory functions and a cancer therapy target. Am J Cancer Res *5*, 2823-2837.

Xie, H., Xu, J., Hsu, J.H., Nguyen, M., Fujiwara, Y., Peng, C., and Orkin, S.H. (2014). Polycomb repressive complex 2 regulates normal hematopoietic stem cell function in a developmental-stage-specific manner. Cell Stem Cell *14*, 68-80.

Zhang, J., Dominguez-Sola, D., Hussein, S., Lee, J.E., Holmes, A.B., Bansal, M., Vlasevska, S., Mo, T., Tang, H., Basso, K.*, et al.* (2015). Disruption of KMT2D perturbs germinal center B cell development and promotes lymphomagenesis. Nat Med *21*, 1190-1198.

Zhang, Y., and Good-Jacobson, K.L. (2019). Epigenetic regulation of B cell fate and function during an immune response. Immunol Rev *288*, 75-84.

Figure 1

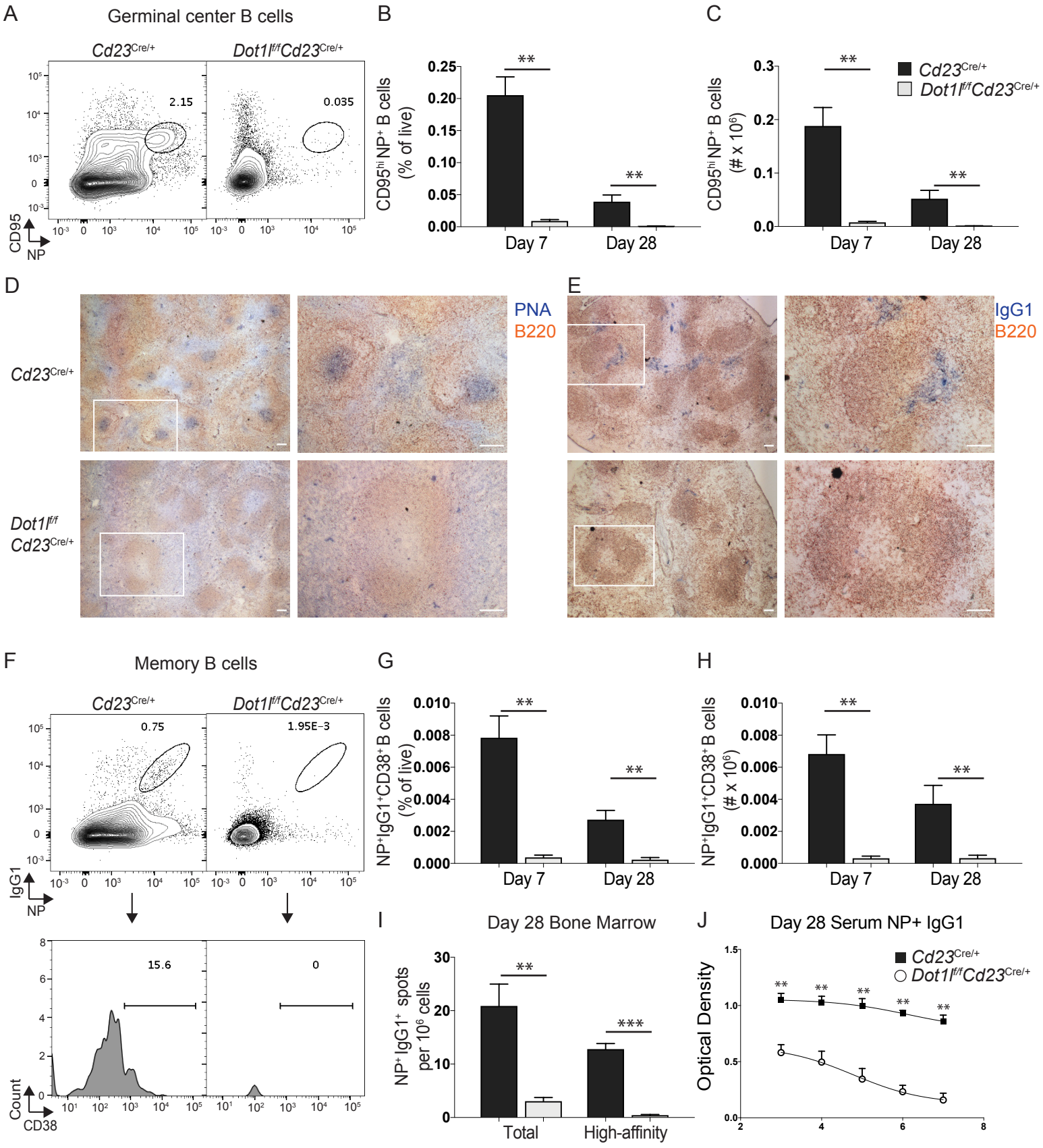

Figure 2

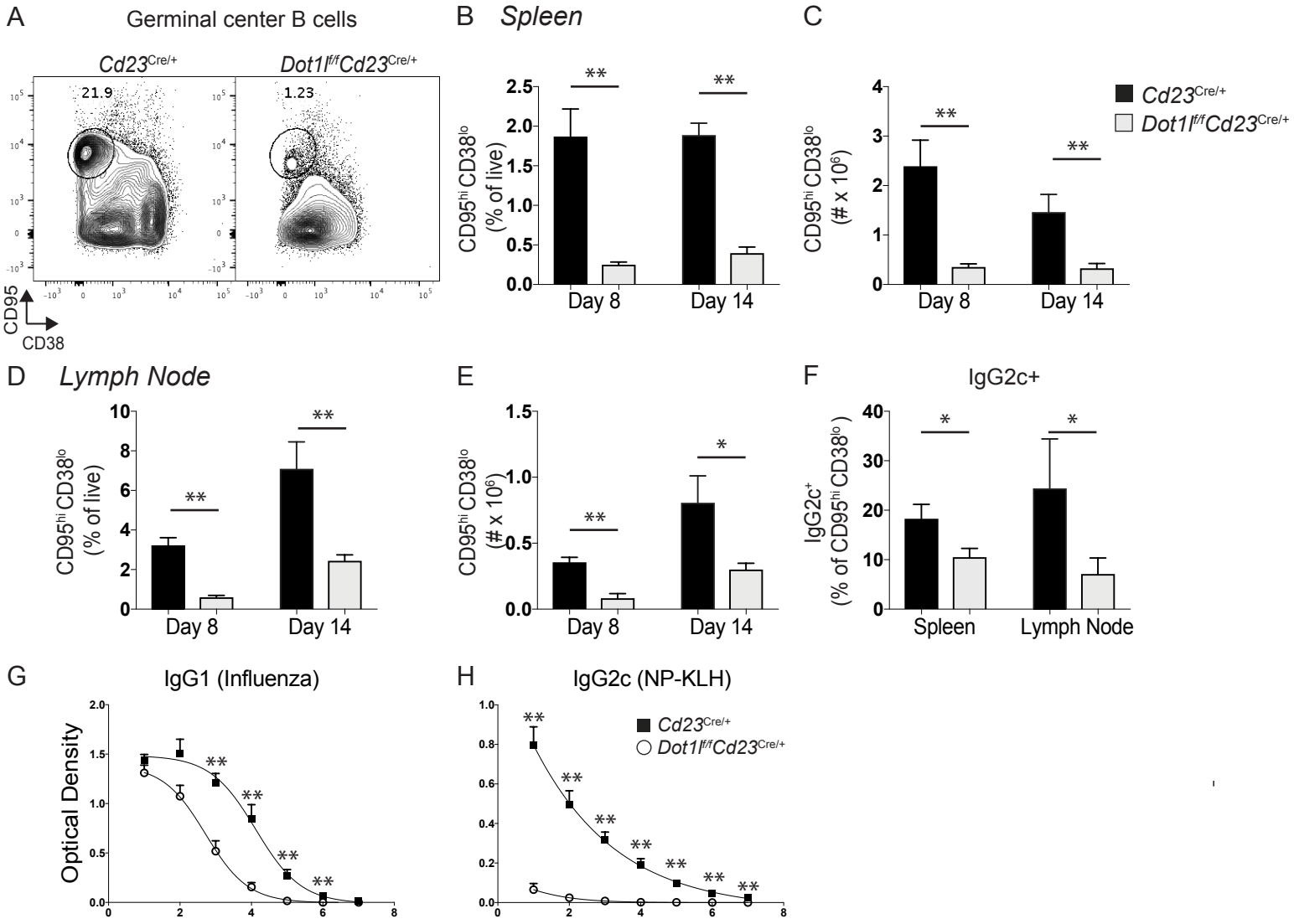

Figure 3

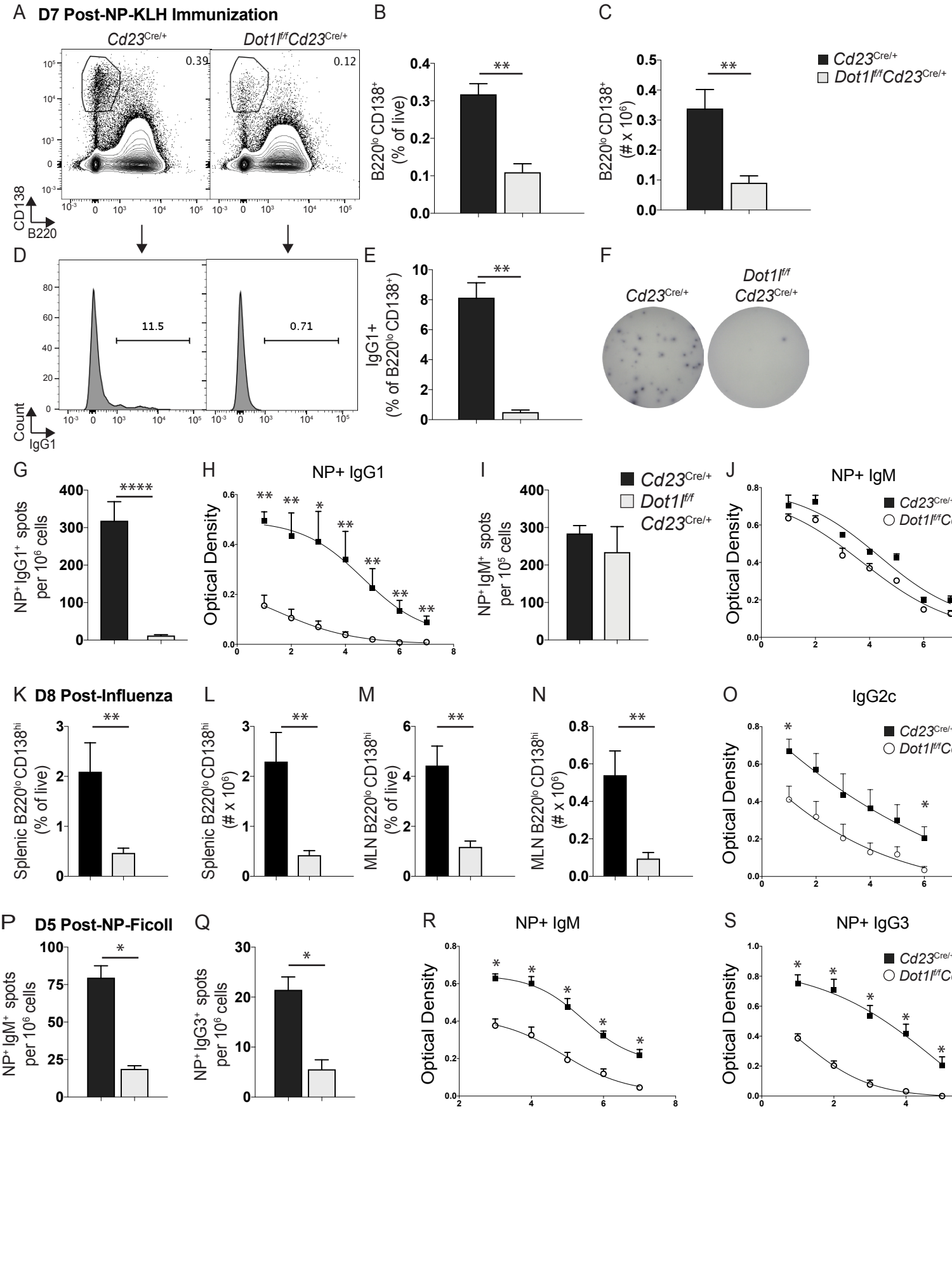

Figure 4

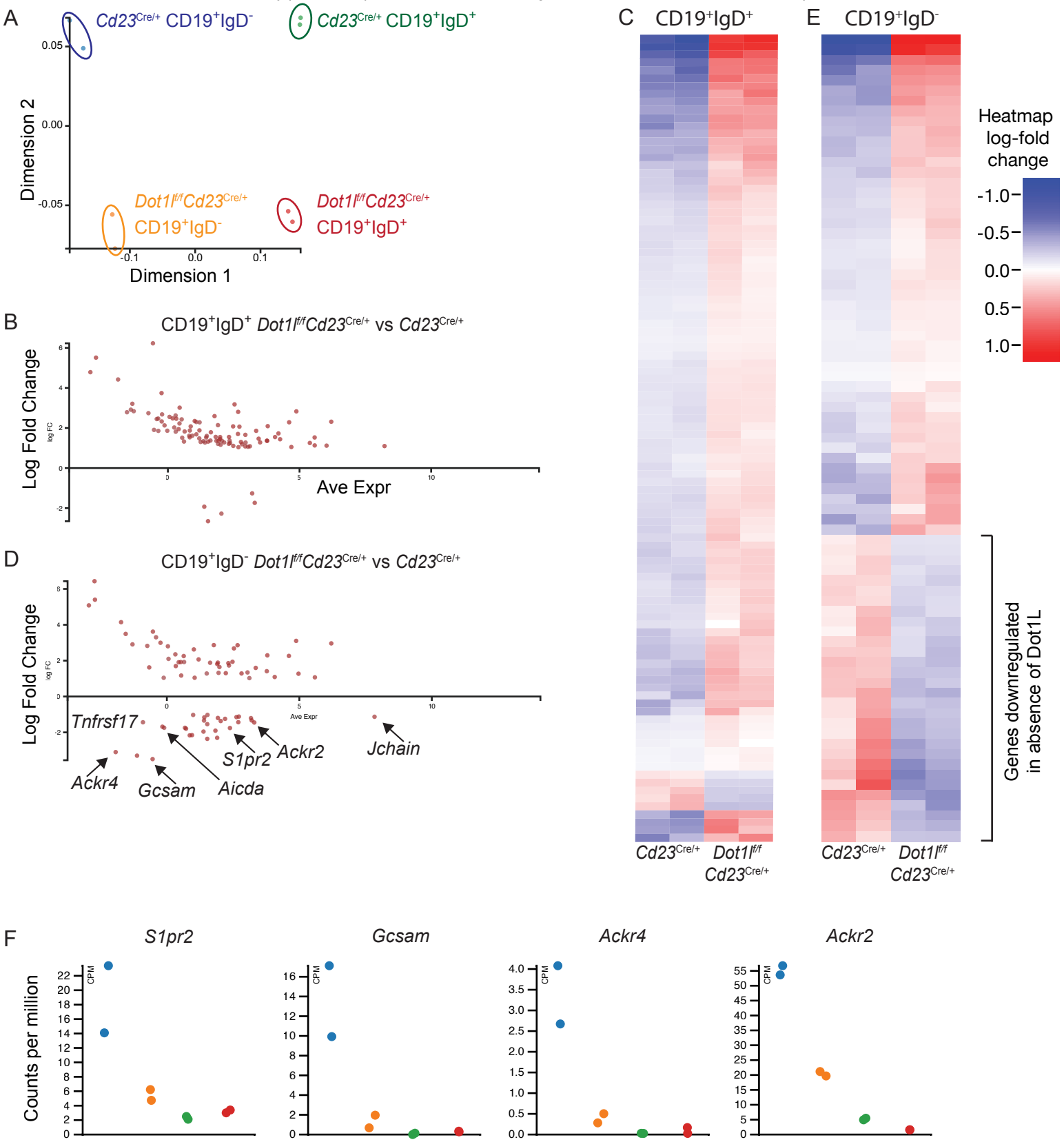

Figure 5

A

Molecular and Cellular Function	# Molecules
Cellular Movement	26
Cell-to-cell Signalling and Interaction	22
DNA Replication, Recombination and Repair	6
Cellular Assembly and Organisation	12
Cell Morphology	15

B

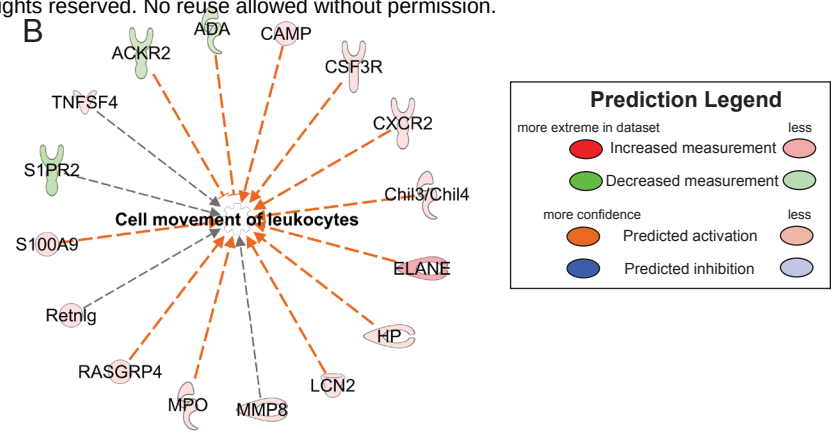

C

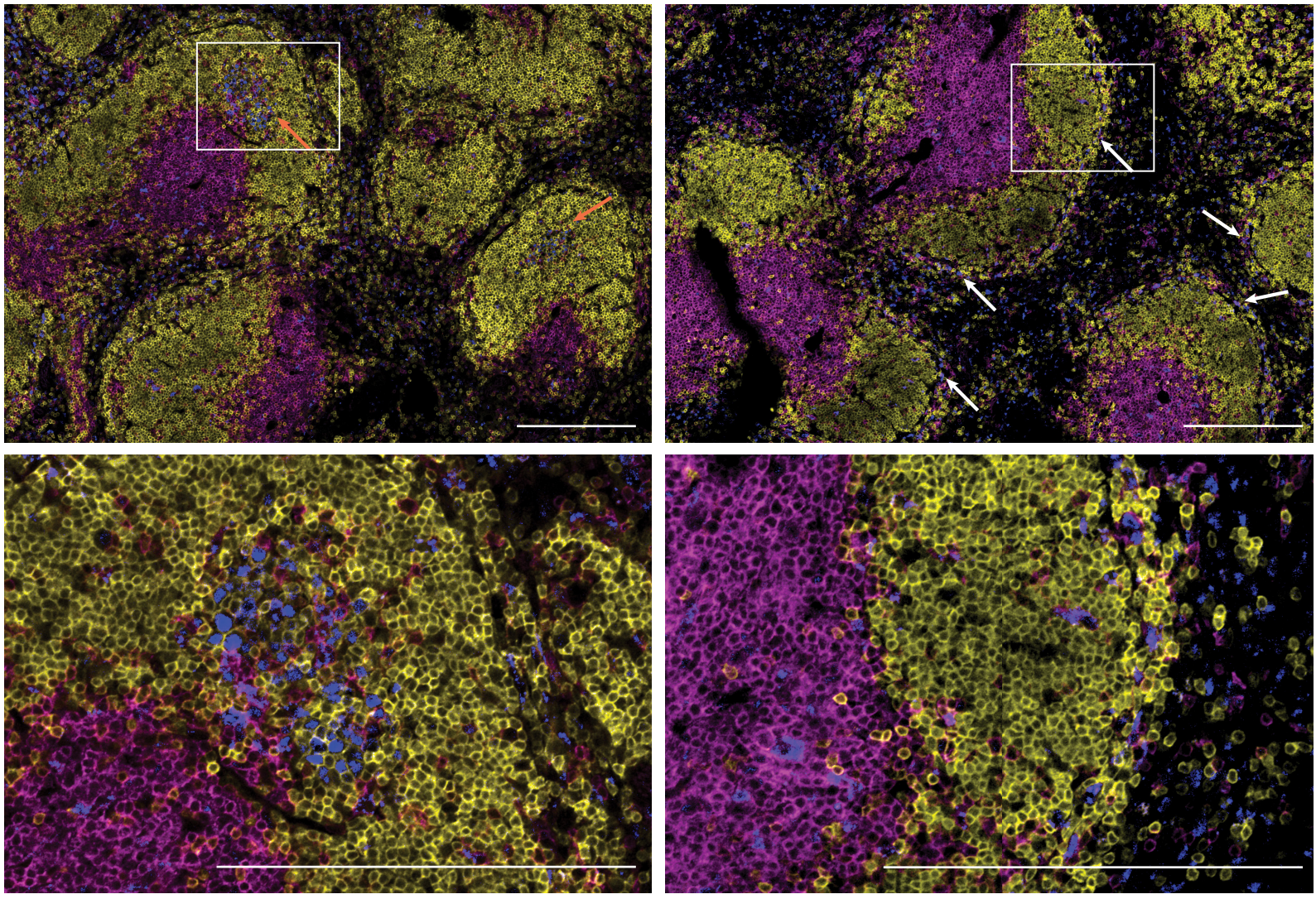

D

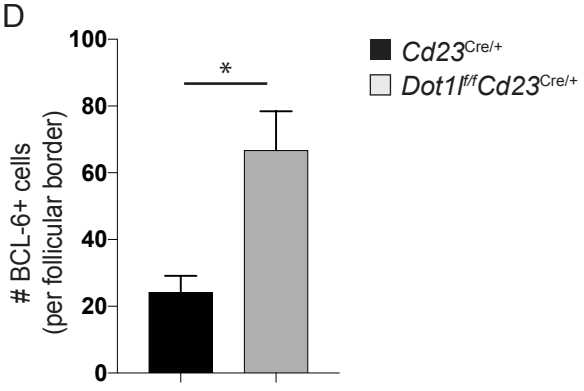

Figure S1

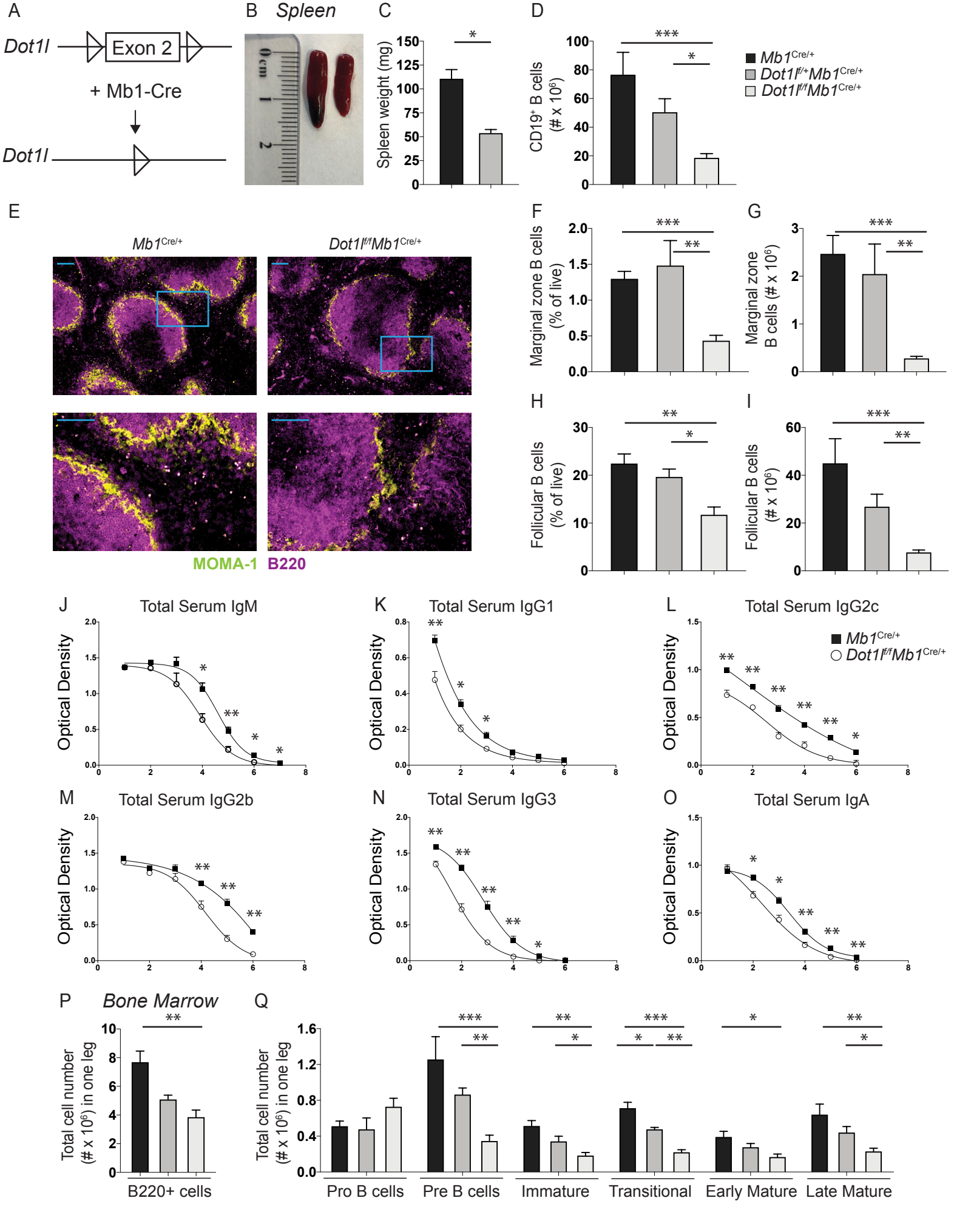

Figure S2

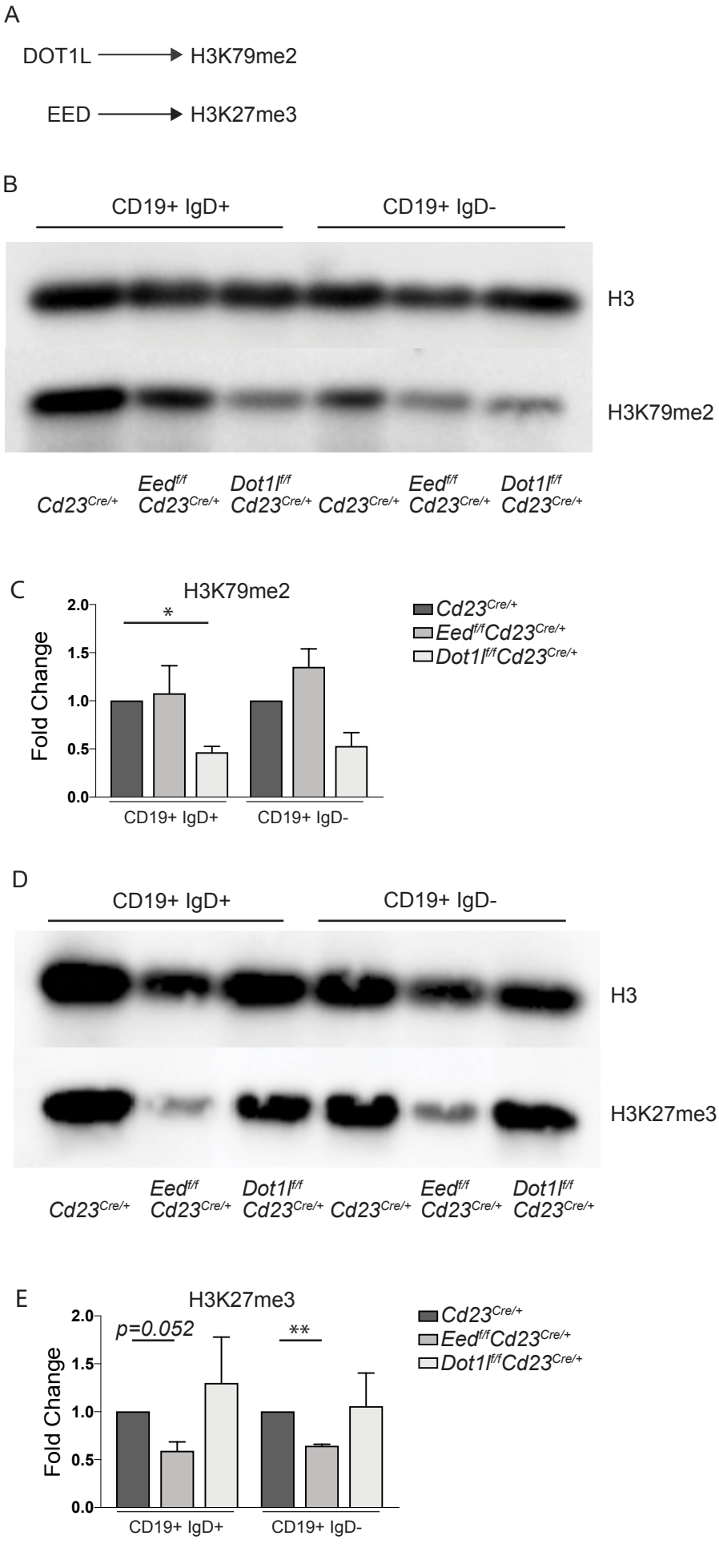

Figure S3

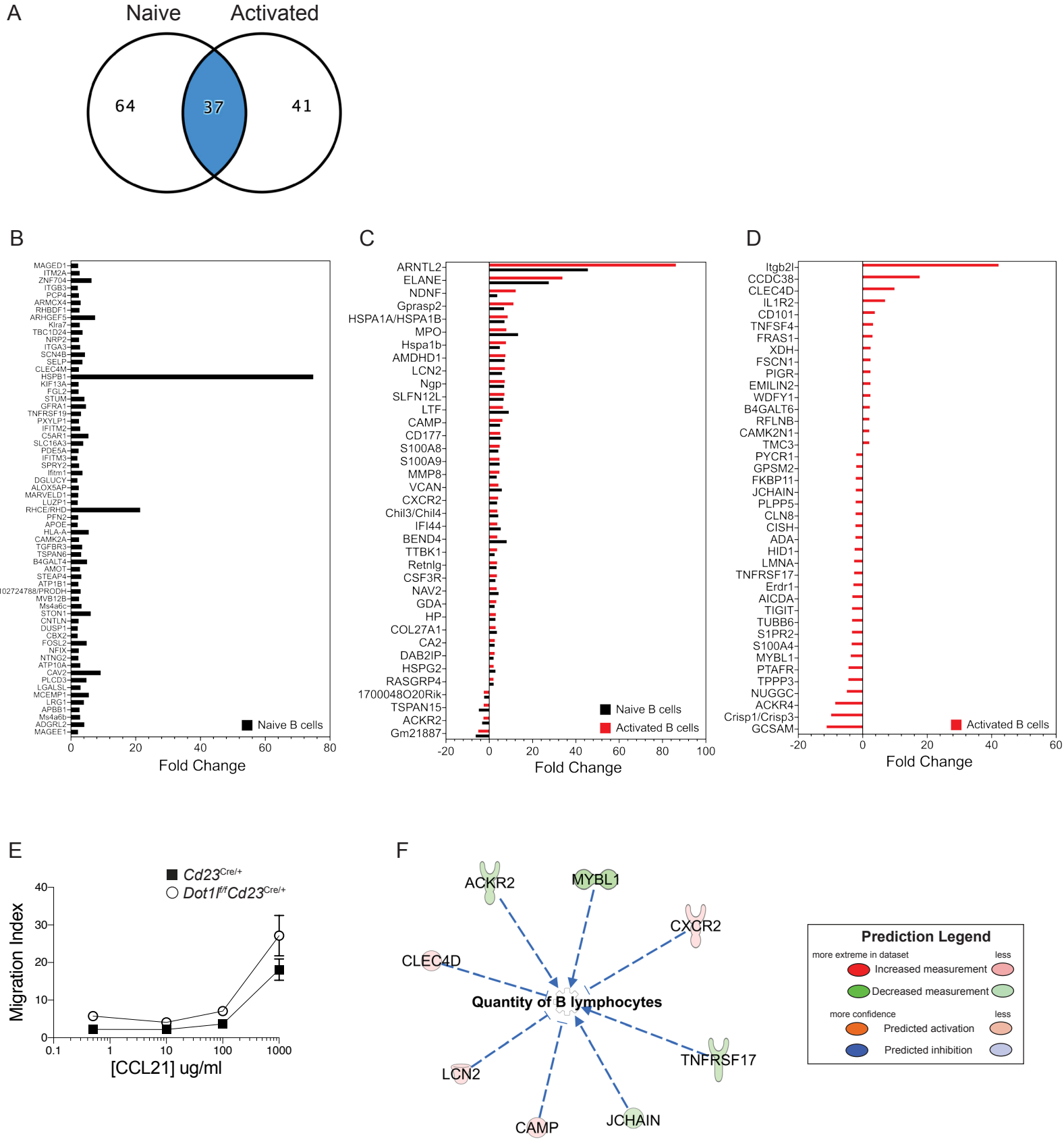

Table S1: Differential gene expression in CD19^{+}IgD^{+} (naïve) B cells. Related to Figure 6.

Gene.Name	Naive-WT	Abs fold change Naive-Dot1L	FDR	AveExpr	P value
Hspa1b	0	2.313857997	3.83E-09	6.205452252	7.51E-13
Hspa1a	0	2.82997678	3.83E-09	4.879616986	3.78E-13
S100a9	0	2.285418632	3.34E-08	4.605694001	9.83E-12
Ms4a6b	0	1.528215408	5.93E-07	5.57400116	2.33E-10
S100a8	0	2.092026557	7.72E-07	3.792594297	4.22E-10
Ngp	0	2.804709673	7.72E-07	2.669183804	4.55E-10
Itgb3	0	1.13041309	9.92E-07	5.576565487	6.81E-10
Ltf	0	3.179306222	1.38282E-06	2.532179342	1.08E-09
Atp1b1	0	1.252418603	2.53446E-06	5.392068551	2.49E-09
Col27a1	0	1.859695931	3.54786E-06	3.353368001	3.83E-09
Rhbdf1	0	1.439365291	1.57856E-05	4.262392664	2.01E-08
9030617O03Rik	0	1.051158964	1.57856E-05	4.689808408	1.97E-08
Lcn2	0	2.591904592	1.66972E-05	1.771857671	2.29E-08
Chil3	0	2.081013798	2.09966E-05	2.477693241	3.09E-08
Ms4a6c	0	1.729239094	5.85118E-05	4.199634789	1.32E-07
Apoe	0	1.0980216	7.70096E-05	8.22855665	2.05E-07
Itm2a	0	1.466180241	7.70096E-05	3.447344365	2.11E-07
Hspg2	0	1.548911188	0.000106919	4.070747525	3.25E-07
Arntl2	0	5.511843755	0.000181506	-2.73078596	6.48E-07
Mpo	0	3.742536309	0.000214381	-0.24037608	7.99E-07
Csf3r	0	1.552258831	0.000228252	2.32150269	8.73E-07
Car2	0	1.360764256	0.000260148	3.77172544	1.13711E-06
Gm21887	0	-2.65104445	0.000315981	1.524836693	1.45642E-06
Camp	0	2.347657962	0.000317715	1.018744522	1.49557E-06
Alox5ap	0	1.302676948	0.000382886	2.776062134	1.9206E-06
Ackr2	0	-1.73638283	0.000656593	3.298832147	3.79906E-06
Kif13a	0	1.281668271	0.00074443	3.502716131	4.38029E-06
Gm21967	0	-1.92678120	0.000906051	1.382477832	5.81321E-06
Steap4	0	1.701807073	0.000906051	2.660848256	5.86441E-06
Ttbk1	0	1.371511953	0.000916656	1.924829065	6.11284E-06
Retnlg	0	1.787442439	0.001017787	1.632434175	6.95379E-06
Cxcr2	0	1.881454752	0.001140607	1.198105702	8.16557E-06
Hp	0	1.548856427	0.001306454	1.983894317	9.73723E-06
Bend4	0	3.014315583	0.001456727	0.446620354	1.1143E-05
Cd177	0	2.462732035	0.001650956	0.320587863	1.39112E-05
Apbb1	0	1.452560022	0.001650956	1.979602247	1.39239E-05
1700048O20Rik	0	-1.26247913	0.001701393	3.20130498	1.4683E-05
Tnfrsf19	0	1.658945857	0.001707939	2.943099025	1.5242E-05

Adgrl2	0	2.066152913	0.00174166	2.717190482	1.57137E-05
Ifitm3	0	1.041676312	0.001857851	2.679912128	1.71264E-05
Mcemp1	0	2.478076436	0.001857851	0.183256946	1.70511E-05
Elane	0	4.785299169	0.002172892	-2.94367441	2.21615E-05
Marveld1	0	1.211773742	0.002172892	2.314742834	2.14306E-05
Dusp1	0	1.119288778	0.002264234	6.027346769	2.35079E-05
Mmp8	0	1.825587502	0.002264234	0.636293431	2.35372E-05
Slc16a3	0	1.943393827	0.002346007	0.409492658	2.5758E-05
Luzp1	0	1.106681635	0.002346007	2.483696189	2.53382E-05
Atp10a	0	1.555034482	0.002394575	1.815360667	2.67708E-05
Tspan6	0	1.683211231	0.002975673	1.081396968	3.70609E-05
B4galt4	0	2.326989425	0.003060935	-0.23441828	4.09806E-05
Tbc1d24	0	1.87470869	0.003060935	0.834015226	4.10647E-05
Cbx2	0	1.08250632	0.003079969	2.938635372	4.16824E-05
Pcp4	0	1.320897754	0.003107206	1.528581734	4.26605E-05
Nrp2	0	1.365526522	0.003206457	3.75968521	4.5281E-05
Rasgrp4	0	1.088839392	0.003988283	3.114169848	5.93773E-05
Scn4b	0	2.1294652	0.003988283	-0.12733163	5.94507E-05
6330403A02Rik	0	2.080020015	0.004101135	0.866337063	6.23395E-05
Hspb1	0	6.226554808	0.004191745	-0.56774818	6.4539E-05
Cav2	0	3.208853709	0.004325722	-1.34952917	6.82986E-05
Vcan	0	2.554364152	0.004531772	0.062317339	7.20832E-05
Nav2	0	2.142143535	0.00462692	1.901764099	7.48693E-05
Cd209a	0	1.323944178	0.00462692	0.611611915	7.45903E-05
Cntln	0	1.27887809	0.004929706	2.136596557	8.2524E-05
Ifitm2	0	1.535979716	0.004929706	0.82902008	8.26694E-05
Itga3	0	1.529484848	0.005228791	1.45404272	9.28127E-05
Maged1	0	1.18784316	0.005228791	2.817588375	9.27159E-05
Amot	0	1.513932927	0.005254769	0.543796854	9.37891E-05
H2-Q10	0	2.470489009	0.00565686	-0.3695914	0.000106255
Gfra1	0	2.22644161	0.00565686	0.440945447	0.000107623
Mvb12b	0	1.359725719	0.00565686	1.840631278	0.000104283
Zfp704	0	2.678941612	0.005774624	-0.22069523	0.00011043
Armcx4	0	1.614749749	0.005789261	0.929017064	0.000111277
Tspan15	0	-2.27358750	0.00580985	2.033337497	0.000115681
Ifi44	0	2.430675976	0.00580985	0.523755385	0.00011463
Rhd	0	4.421461976	0.00580985	-1.89216823	0.000113425
Magee1	0	1.162911915	0.005939235	2.003540417	0.000120567
Klra1	0	1.480750803	0.006004832	1.193340345	0.000122488
Ifitm1	0	1.864346011	0.006216178	-0.02196145	0.000128018
Fgl2	0	1.274622624	0.006622455	2.95040722	0.000140062
Slfn4	0	2.741002326	0.006774663	-0.73901729	0.000146258

Nfix	0	1.303990551	0.006774663	1.245153007	0.000147492
Lrg1	0	2.023849417	0.006899636	0.242023401	0.000150889
Gda	0	1.368179881	0.007218036	2.344464388	0.000164223
Spry2	0	1.373857297	0.007411651	1.615658306	0.000171536
Dab2ip	0	1.063512918	0.007602159	3.0441097	0.00017669
Lgalsl	0	1.60319526	0.00764702	1.476208954	0.000180733
Camk2a	0	1.360303528	0.00764702	2.052113313	0.000180453
C5ar1	0	2.447922829	0.007694422	-0.42316542	0.000182608
Ndnf	0	1.905522971	0.00796378	-0.52665119	0.000194946
Prodh	0	1.615569057	0.00811799	0.812653497	0.000201417
Pde5a	0	1.274629829	0.008192762	1.409352637	0.000206486
Amdhd1	0	2.83971926	0.008240736	-1.29764159	0.000208503
Plcd3	0	2.282749986	0.008803824	1.204021593	0.000228794
Tgfbr3	0	1.814568533	0.008897631	0.297436996	0.00023332
Selp	0	1.856638972	0.009014327	-0.36317281	0.000240425
Ston1	0	2.625886405	0.009130206	0.293250105	0.000247564
Pxylp1	0	1.340622999	0.009408159	1.350176515	0.000258339
Gprasp2	0	2.786865511	0.009537935	-1.55393697	0.000262838
Pfn2	0	1.208075063	0.009556168	1.90405161	0.000264278
Arhgef5	0	2.914275509	0.009566016	-1.40633817	0.000265488
Ntng2	0	1.249239098	0.009687143	2.364384356	0.0002698
Fosl2	0	2.299255193	0.009973047	1.079428364	0.000279389

Table S2: Differential gene expression in CD19^{+}IgD^{-} B cells. Related to Figure 6.

Gene.Name	Act-WT	Abs Fold Change Act-Dot1L	FDR	AveExpr	P value
Hspa1b	0	2.963011017	4.34E-10	6.205452252	8.06E-14
Hspa1a	0	3.102334636	4.34E-10	4.879616986	8.51E-14
Ackr2	0	-1.450772663	1.34E-07	3.298832147	3.94E-11
S100a9	0	2.263724375	1.51E-07	4.605694001	5.91E-11
Ngp	0	2.860646155	1.52148E-06	2.669183804	7.46E-10
S100a8	0	2.296262808	2.79486E-06	3.792594297	1.64E-09
Wdfy1	0	1.271289152	6.0492E-06	4.96865679	4.15E-09
Ltf	0	2.683125266	1.22118E-05	2.532179342	9.58E-09
Tspan15	0	-1.367851595	1.45721E-05	2.033337497	1.29E-08
Lcn2	0	2.86545773	3.00007E-05	1.771857671	3.81E-08
Col27a1	0	1.595863026	3.00007E-05	3.353368001	3.82E-08
Mybl1	0	-1.905282256	3.05435E-05	1.832856284	4.21E-08
Lmna	0	-1.432948032	3.15025E-05	2.69732882	5.17E-08
Tppp3	0	-2.167100014	3.35676E-05	0.863801565	6.25E-08
Arntl2	0	6.43013515	4.69155E-05	-2.73078596	9.27E-08
Chil3	0	1.936405848	6.58345E-05	2.477693241	1.49E-07
1700048O20Rik	0	-1.333227954	7.51845E-05	3.20130498	1.84E-07
Cish	0	-1.197333307	7.85334E-05	1.925283523	2.08E-07
Ptafr	0	-2.155105866	8.03163E-05	0.94943737	2.28E-07
Fscn1	0	1.300791748	8.03163E-05	2.224109896	2.22E-07
Nav2	0	1.811790407	8.27242E-05	1.901764099	2.51E-07
Nuggc	0	-2.305016236	9.37958E-05	1.898574667	3.04E-07
Itgb2l	0	5.398933447	0.000112991	-2.71417215	3.90E-07
Tnfsf4	0	1.697711699	0.000151561	0.336927158	5.56E-07
Pigr	0	1.285121108	0.000155526	2.818614997	6.31E-07
Gm21887	0	-2.360590592	0.000283807	1.524836693	1.32649E-06
Csf3r	0	1.860464851	0.000365817	2.32150269	1.90137E-06
Camp	0	2.625197311	0.000393741	1.018744522	2.17399E-06
Aicda	0	-1.685516964	0.000399143	-0.16864192	2.2703E-06
Fras1	0	1.622493896	0.000401568	-0.66645710	2.32348E-06
Tubb6	0	-1.745082994	0.000632179	0.682645537	3.87853E-06
Osgin1	0	-1.245300231	0.000632179	2.197293988	3.90579E-06
S1pr2	0	-1.756991175	0.000804046	2.380981776	5.04648E-06
Crisp1	0	-3.300227456	0.000934408	-1.12595260	6.3799E-06
Hspg2	0	1.088707641	0.000934408	4.070747525	6.46449E-06
Ppapdc1b	0	-1.14898672	0.000934408	2.62607476	6.25076E-06
Gcsam	0	-3.490270123	0.00101548	-0.53863487	7.36937E-06
Fkbp11	0	-1.119574903	0.001126245	2.717657325	8.50455E-06

S100a4	0	-1.796461884	0.001379105	0.723824301	1.1211E-05
Cln8	0	-1.163385706	0.001532173	1.413029855	1.33729E-05
Mmp8	0	2.255963928	0.001532173	0.636293431	1.31669E-05
Ackr4	0	-3.10011899	0.001532173	-1.93229685	1.32916E-05
Cxcr2	0	2.069240736	0.001597484	1.198105702	1.40996E-05
Gm21967	0	-1.956898624	0.001822012	1.382477832	1.73791E-05
Ndnf	0	3.618676879	0.001822012	-0.52665119	1.75108E-05
Ccdc38	0	4.144568256	0.001868973	-1.72777374	1.83287E-05
Elane	0	5.082166094	0.001955334	-2.94367441	1.99426E-05
Gprasp2	0	3.490883479	0.001955334	-1.55393697	1.97794E-05
Fam101b	0	1.069817226	0.002037602	5.587118514	2.20299E-05
Mpo	0	2.997407607	0.002081724	-0.24037608	2.3069E-05
Ada	0	-1.206160768	0.002158388	3.173973269	2.76771E-05
Car2	0	1.410336274	0.002158388	3.77172544	2.62527E-05
Ifi44	0	1.920036673	0.002158388	0.523755385	2.76128E-05
Camk2n1	0	1.04577939	0.002158388	1.04838751	2.59448E-05
Ttbk1	0	1.889412322	0.002343803	1.924829065	3.03405E-05
B4galt6	0	1.169611758	0.00243601	0.540855937	3.24233E-05
Jchain	0	-1.130510644	0.002999923	7.83805826	4.38353E-05
Hp	0	1.643155577	0.003035657	1.983894317	4.49369E-05
Hid1	0	-1.340404776	0.003359416	1.402147505	5.17239E-05
Amdhd1	0	2.907492533	0.003553253	-1.29764159	5.57537E-05
Retnlg	0	1.882665812	0.003690474	1.632434175	5.9347E-05
Erdr1	0	-1.541826294	0.003742839	1.52555859	6.05637E-05
Cd177	0	2.351722309	0.004053177	0.320587863	6.71753E-05
Il1r2	0	2.801296244	0.004134054	0.039072859	6.93266E-05
Bend4	0	1.910190155	0.004348129	0.446620354	7.63278E-05
Gpsm2	0	-1.027515451	0.004644209	0.991933497	8.39913E-05
Gda	0	1.729824062	0.004762996	2.344464388	8.73473E-05
Slfn4	0	2.82326356	0.005472365	-0.73901729	0.00010626
Xdh	0	1.318491944	0.005698344	1.951240169	0.000111206
Pycr1	0	-1.025345269	0.0059004	1.533510018	0.000119779
Tnfrsf17	0	-1.437967394	0.006140709	-0.90241905	0.000127737
Dab2ip	0	1.342662908	0.006140709	3.0441097	0.00012634
Clec4d	0	3.303470614	0.006557919	-0.40873811	0.000139558
Vcan	0	2.099137248	0.007772043	0.062317339	0.00018445
Tigit	0	-1.743921519	0.00853285	-0.10225920	0.000211932
Cd101	0	1.923702091	0.008766411	0.65004755	0.000224383
Emilin2	0	1.28263613	0.009539102	1.504554161	0.000250709
Rasgrp4	0	1.026352151	0.009909572	3.114169848	0.000273079
Tmc3	0	1.042977263	0.009909572	-0.11885847	0.000270808

Table S3: Antibodies and reagents.

REAGENT or RESOURCE	SOURCE
Anti-CD138 PE (clone 281-2)	BioLegend
Anti-CD138 BV605 (clone 281-2)	BD Bioscience
Anti-CD45R (B220) AF488 (clone RA3-6B2)	BioLegend
Anti-CD45R (B220) APC-Cy7 (clone RA3-6B2)	BioLegend
Anti-CD45R (B220) AF555 (clone RA3-6B2)	Produced in-house
Anti-IgG1 APC (clone X56)	BD Bioscience
Anti-CD19 APC-Cy7 (clone 6D5)	BioLegend
Anti-CD19 Pacific Blue (clone 6D5)	BioLegend
Anti-CD19 PE (clone 6D5)	BioLegend
Anti-IgD AF488 (clone 11-26c.2a)	BioLegend
Anti-IgD PerCP-Cy5.5 (clone 11-26c.2a)	BD Bioscience
Anti-CD95 PE-Cy7 (clone Jo2)	BD Bioscience
Anti-CD38 Pacific Blue (clone 90)	BioLegend
Anti-IgG2a/2b FITC (clone R2-40)	BD Bioscience
Anti-CD43 APC (clone S11)	BioLegend
Anti-CD249 (BP1) PE (clone BP-1)	BD Bioscience
Anti-CD24 BV421(clone M1/69)	BioLegend
Anti-IgM AF488 (clone RMM-1)	BioLegend
Anti-CD169 (MOMA-1) FITC (clone 3D6.112)	Bio-Rad
Anti-CD23 AF488 (clone B3B4)	BioLegend
Anti-CD21/CD35 APC (clone 7G6)	BioLegend
Anti-CD11b APC-Cy7 (clone M1/70)	TONBO
Anti-CD3e PE-Cy7 (clone 145-2C11)	eBioscience
Anti-CD4 A488 (clone GK1.5-7)	Produced in-house

Anti-CD8a A488 (clone 53.6.7)	Produced in-house
Anti-Bcl6 A647 (clone K112-91)	BD Pharmingen
Goat anti-mouse IgG1 unlabeled (polyclonal)	Southern Biotech
Goat anti-mouse IgG2a unlabeled (polyclonal)	Southern Biotech
Goat anti-mouse IgG2b unlabeled (polyclonal)	Southern Biotech
Goat anti-mouse IgG3 unlabeled (polyclonal)	Southern Biotech
Goat anti-mouse IgA unlabeled (polyclonal)	Southern Biotech
Goat anti-mouse IgM unlabeled (polyclonal)	Southern Biotech
Goat anti-mouse IgG1 HRP (polyclonal)	Southern Biotech
Goat anti-mouse IgG2a HRP (polyclonal)	Southern Biotech
Goat anti-mouse IgG2c HRP (polyclonal)	Southern Biotech
Goat anti-mouse IgG2b HRP (polyclonal)	Southern Biotech
Goat anti-mouse IgG3 HRP (polyclonal)	Southern Biotech
Goat anti-mouse IgA HRP (polyclonal)	Southern Biotech
Goat anti-mouse IgM HRP (polyclonal)	Southern Biotech
Goat anti-mouse IgG3 AP (polyclonal)	Southern Biotech
Goat anti-mouse IgG1 AP (polyclonal)	Southern Biotech
Goat anti-mouse IgM AP (polyclonal)	Southern Biotech
Rat anti-mouse CD45R (B220) (clone RA3-6B2)	BD Pharmingen
AffiniPure Goat Anti-Rat IgG (H+L) (polyclonal)	Jackson Laboratory
Streptavidin Alkaline Phosphatase	Southern Biotech
Anti-H3 (polyclonal)	Abcam
Anti-H3K27me3 (clone 6002)	Abcam
Anti-H3K79me2 (polyclonal)	Abcam
AffiniPure Goat Anti-Rabbit IgG (H+L) HRP (polyclonal)	Southern Biotech
AffiniPure Goat Anti-Mouse IgG (H+L) HRP (polyclonal)	Biorad

NP-PE	Conjugated in-house
Peanut Agglutinin	Vector Laboratories
BD Cytofix™	BD Biosciences
Clarity Max™ Western ECL Substrate	Biorad
O.C.T Compound	Tissue-Tek
Fixable Viability Stain 700	BD Horizon
AEC Peroxidase (HRP) Substrate Kit	Vector Laboratories
Vector® Blue Alkaline Phosphatase Substrate Kit	Vector Laboratories